# Ruthenium(II) as a Novel Labile Partner in Thermodynamic Self-Assembly of Heterobimetallic d–f Triple-Stranded Helicates

**Stéphane Torelli,[a] Sandra Delahaye,[b] Andreas Hauser,[b] Gérald Bernardinelli,[c] and Claude Piguet*[a]**

**Abstract:** Unsymmetrical substituted bidentate benzimidazol-2-ylpyridine ligands L2 and L3 react with [Ru(dmso)$_4$Cl$_2$] in ethanol to give statistical 1:3 mixtures of *fac*-[Ru(L*i*)$_3$]$^{2+}$ and *mer*-[Ru(L*i*)$_3$]$^{2+}$ ($i=2$, 3; $\Delta G^{\ominus}_{\text{isomerisation}} = -2.7\ \text{kJ mol}^{-1}$). In more polar solvents (acetonitrile, methanol), the free energy of the facial⇌meridional isomerisation process favours *mer*-[Ru(L*i*)$_3$]$^{2+}$, which is the only isomer observed in solution at the equilibrium ($\Delta G^{\ominus}_{\text{isomerisation}} \leq -11.4\ \text{kJ mol}^{-1}$). Since the latter process takes several days for [Ru(L2)$_3$]$^{2+}$, *fac*-[Ru(L2)$_3$]$^{2+}$ and *mer*-[Ru(L2)$_3$]$^{2+}$ have been separated by chromatography, but the 28-fold increase in velocity observed for [Ru(L3)$_3$]$^{2+}$ provides only *mer*-[Ru(L3)$_3$](ClO$_4$)$_2$ after chromatography ($RuC_{60}H_{51}N_9O_8Cl_2$, monoclinic, $P2_1/n$, $Z=4$). The facial isomer can be stabilised when an appended tridentate binding unit, connected at the 5-position of the benzimidazol-2-ylpyridine unit in ligand L1, interacts with nine-coordinate lanthanides(III). The free energy of the facial⇌meridional isomerisation is reversed ($\Delta G^{\ominus}_{\text{isomerisation}} \geq 11.4\ \text{kJ mol}^{-1}$), and the Ru–N bonds are labile enough to allow the quantitative thermodynamic self-assembly of *HHH*-[RuLu(L1)$_3$]$^{5+}$ within hours ([RuLu(L1)$_3$](CF$_3$SO$_3$)$_{4.5}$Cl$_{0.5}$(CH$_3$OH)$_{2.5}$: $RuLuC_{106}H_{109}Cl_{0.5}N_{21}O_{19}S_{4.5}F_{13.5}$, triclinic, $P\bar{1}$, $Z=2$). Electrochemical and photophysical studies show that the benzimidazol-2-ylpyridine units in L1–L3 display similar π-acceptor properties to, but stronger π-donor properties than, those found in 2,2′-bipyridine. This shifts the intraligand $\pi\rightarrow\pi^*$ and the MLCT transitions toward lower energies in the pseudo-octahedral [Ru(L*i*)$_3$]$^{2+}$ ($i=2$, 3) chromophores. The concomitant short lifetime of the $^3$MLCT excited state points to efficient, thermally activated quenching via low-energy Ru-centred d–d states, a limitation which is partially overcome by mechanical coupling in *HHH*-[RuLu(L1)$_3$]$^{5+}$.

**Keywords:** helical structures · isomerization · lanthanides · ruthenium · self-assembly

[a] Dr. S. Torelli, Prof. Dr. C. Piguet
Department of Inorganic, Analytical and Applied Chemistry
University of Geneva, 30 quai E. Ansermet
1211 Geneva 4 (Switzerland)
Fax: (+41) 22-379-6830
E-mail: Claude.Piguet@chiam.unige.ch

[b] S. Delahaye, Prof. Dr. A. Hauser
Department of Physical Chemistry
University of Geneva, 30 quai E. Ansermet
1211 Geneva 4 (Switzerland)

[c] Dr G. Bernardinelli
Laboratory of X-ray Crystallography
University of Geneva, 24 quai E. Ansermet
1211 Geneva 4 (Switzerland)

Supporting information for this article is available on the WWW under http://www.chemeurj.org/ or from the author. $^1$H NMR data for complexes **1**–**3** are collected in Table S1, while Tables S2–S4 list selected structural parameters for the metallic coordination spheres in **4** and **6**. Figure S1 shows plots of ln(|fac(*t*)|) versus *t* for [Ru(L2)$_3$]$^{2+}$ and [Ru(L3)$_3$]$^{2+}$; Figures S2 and S5 display the packing of the cations in the crystal structures of **4** and **6**. Figure S3 shows photophysical data for [RuLu(L1)$_3$]$^{5+}$ in solution, Figure S4 exhibits an optimised superimposition of the molecular structures of [RuLu(L1)$_3$]$^{5+}$ and [CoLu(L1)$_3$]$^{6+}$, and Figure S6 displays variable-temperature $^1$H NMR spectra for [Zn(L2)$_3$]$^{2+}$ and [Zn(L3)$_3$]$^{2+}$.

## Introduction

Kinetically inert, pseudo-octahedral [Ru(α,α′-diimine)$_3$]$^{2+}$ building blocks such as [Ru(2,2′-bipyridine)$_3$]$^{2+}$ and its derivatives are used universally for inducing specific photophysical and electrochemical properties in coordination complexes.[1] Of particular interest is their introduction into metallosupramolecular polymetallic functional artificial photosynthetic systems in which electrons are directed towards specific sites in order to perform light-activated secondary reactions.[2] In a closely related context, Klink et al. demonstrated that [Ru(2,2′-bipyridine)$_3$]$^{2+}$ can be used as an efficient photosensitiser for lanthanide-centred near-infrared emission (Ln = Nd, Yb) occurring after intramolecular intermetallic 4d→4f energy transfer.[3] When $C_2$-symmetrical bidentate α,α′-diimine ligands are used, a single pair of inert helical enantiomers results (*P*-[Ru(α,α′-diimine)$_3$]$^{2+}$ and *M*-[Ru(α,α′-diimine)$_3$]$^{2+}$), which can be separated after interaction with enantiomerically pure counter-anions.[4] However, for bidentate ligands L with two different donor sites, the tris-chelates may exist as two pairs of helical enantiomers:

 **DOI: 10.1002/chem.200400092** © 2004 Wiley-VCH Verlag GmbH & Co. KGaA, Weinheim 

*P-fac*-$[Ru(L)_3]^{2+}$/*M-fac*-$[Ru(L)_3]^{2+}$ and *P-mer*-$[Ru(L)_3]^{2+}$/*M-mer*-$[Ru(L)_3]^{2+}$, in which *fac* stands for the $C_3$-symmetrical facial isomer (three ligands with parallel orientations) and *mer* characterises the $C_1$-symmetrical meridional isomer (one ligand adopts the opposite orientation).[5] Although the separation of *fac*/*mer* isomers on the laboratory scale has been reported together with different spectroscopic properties for each isomer,[6] it is only recently that pure facial isomers have been designed for further functionalisation and incorporation into stereocontrolled molecular architectures.[7] Following our interest in the design of the triple-stranded d–f helicates $[MLn(L1)_3]^{6+}$ (Figure 1) in which the d-block ion (M = $Cr^{III}$, $Co^{III}$) is inert enough to provide the chiral facial receptors *fac*-$[M(L1)_3]^{3+}$ upon decomplexation of $Ln^{III}$,[8,9] we plan to investigate the introduction of inert 4d-block $Ru^{II}$ ions as partners in strict self-assembly processes. Such a challenging approach has been developed successfully for $Co^{III}$[8] and $Cr^{III}$,[9] because they possess reduced forms ($Co^{II}$ and $Cr^{II}$) which exhibit similar stereochemical preferences but which are labile enough to allow the exploration of the energy hypersurface of the assembly process, before undergoing oxidative post-modification leading to the final inert architectures.[10] Interestingly, *fac*-$[Cr(L1)_3]^{3+}$ can be separated into its helical *P* and *M* enantiomers to give dual $Cr^{III}$ and $Eu^{III}$-centred circularly polarised emission after recombination in the chiral *PP*-$[CrEu(L1)_3]^{6+}$ and *MM*-$[CrEu(L1)_3]^{6+}$ helicates.[11] Moreover, the specific photophysical properties of *fac*-[Cr(benzimidazol-2-ylpyridine$)_3]^{3+}$ have been exploited for sensitizing long-lived near-infrared emission in *rac*-$[CrLn(L1)_3]^{6+}$ (Ln = Nd, Yb).[12] However, the long electronic relaxation of paramagnetic $Cr^{III}$ combined with its high positive charge strongly limits the structural characterisation (NMR spectroscopy) and the stability of the inert helicates $[CrLn(L1)_3]^{6+}$ in solution. *fac*-[Ru(benzimidazol-2-ylpyridine$)_3]^{2+}$ thus corresponds to an attractive compromise displaying 1) photophysical properties compatible with intramolecular intermetallic 4d–4f energy transfer processes in $[RuLn(L1)_3]^{5+}$, 2) a diamagnetic $^1A_1$ (low-spin $4d^6$) ground state compatible with efficient structural characterisation in solution by NMR techniques and c) a small 2+ charge which reduces intermetallic electrostatic repulsion in the final helicates. However, the related $[Ru^{III}(\alpha,\alpha'\text{-diimine})_3]^{3+}$ is too oxidizing and kinetically inert[13] to be used as a precursor in strict self-assembly processes with lanthanides and L1, and the introduction of inert $Ru^{II}$ cannot take advantage of reductive post-modification of an $Ru^{III}$ analogue. Encouraged by the 57% yield reported for the formation of $[(Cu^{I})_3\{fac\text{-}Ru^{II}(\text{pyridine-pyrazolate})_3\}_2]^{-}$, which implies quite a fast (that is, on the time scale of an hour) *fac*-$[Ru^{II}(\text{pyridine-pyrazolate})_3]^{-}$⇌*mer*-$[Ru^{II}(\text{pyridine-pyrazolate})_3]^{-}$ process,[14] we have explored the factors that could be responsible for the tuning of the lability in pseudo-octahedral [Ru(benzimidazol-2-ylpyridine$)_3]^{2+}$ in order to induce strict self-assembly between L1, $Ln^{III}$, and $Ru^{II}$. We report in this paper the kinetic and thermodynamic properties of the facial⇌meridional isomerisation process occurring in $[Ru(Li)_3]^{2+}$ ($i$ = 2, 3), together with the first introduction of the 4d-block $Ru^{II}$ cation into the d–f helicate $[RuLu(L1)_3]^{5+}$. Particular attention is also focused on the photophysical properties of the $Ru^{II}$ centrs in these complexes for the future induction of directional light-conversion processes in luminescent heterobimetallic helicates.

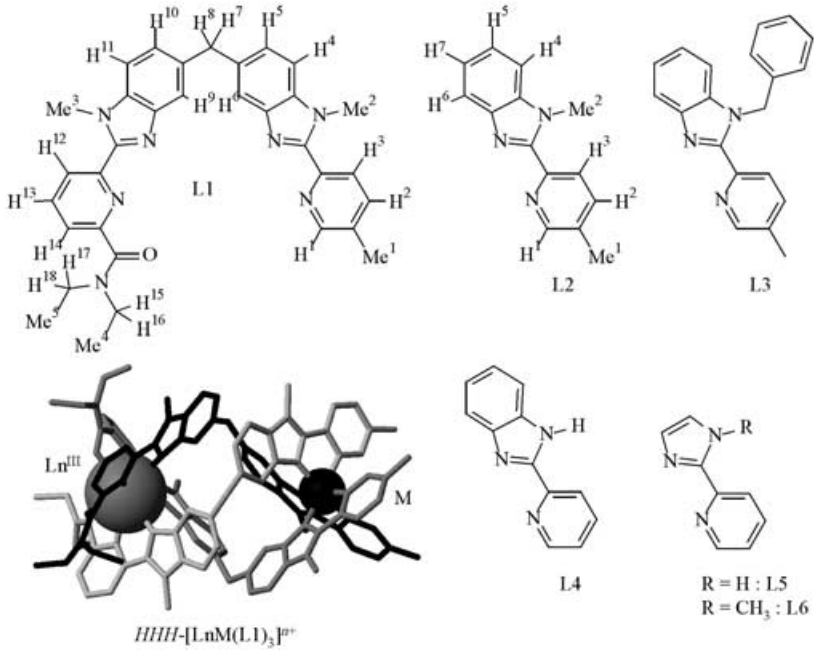


Figure 1. Structures of the ligands L1–L6, and of the heterobimetallic d–f triple-stranded helicates *HHH*-$[LnM(L1)_3]^{n+}$ (the crystal structure of *HHH*-$[LuCr(L1)_3]^{6+}$ is represented here).[9]

## Results and Discussion

**Preparation and characterisation of *mer*-$[Ru(L2)_3](ClO_4)_2\cdot 2H_2O$ (1), *fac*-$[Ru(L2)_3](ClO_4)_2\cdot 2H_2O$ (2) and *mer*-$[Ru(L3)_3](ClO_4)_2\cdot CH_3CN\cdot H_2O$ (3)**: The bidentate ligand L2 was obtained according to a literature procedure[15] in which the reductive cyclisation of an *ortho*-nitroarene–carboxamide precursor provides the substituted benzimidazole ring as the key step.[16] The same strategy was used for the synthesis of L3, which was obtained in good yield (90%) (Scheme 1). Refluxing L*i* ($i$ = 2, 3; 3 equiv) with [Ru(dmso$)_4Cl_2$] (1 equiv) in ethanol for 24 h followed by metathesis with $NaClO_4$ and precipitation from acetonitrile/diethyl ether provided $[Ru(L2)_3](ClO_4)_2\cdot 2H_2O$ and $[Ru(L3)_3](ClO_4)_2\cdot CH_3CN\cdot H_2O$ in 56% and 72% yield, respectively.


© 2004 Wiley-VCH Verlag GmbH & Co. KGaA, Weinheim

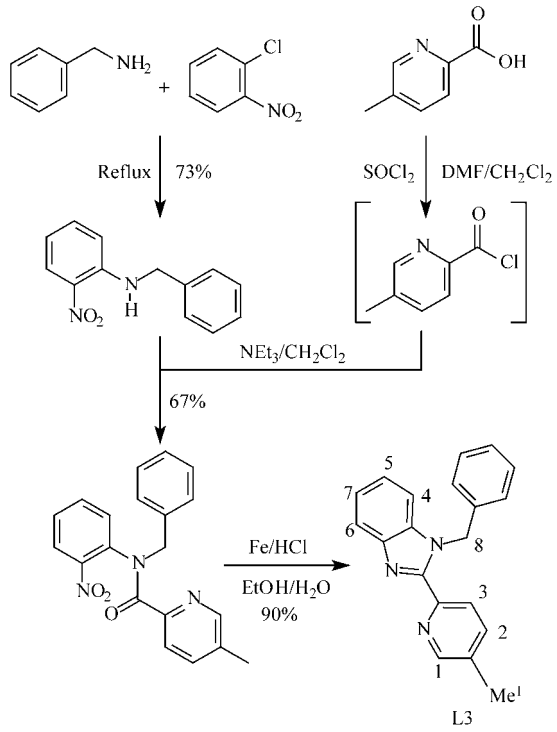


Scheme 1. Synthesis of L3.

The $^1$H NMR spectra of these complexes in $CD_3CN$, recorded immediately after solubilisation of the solid samples, were characteristic of statistical 1:3 mixtures of *fac*-$[Ru(Li)_3]^{2+}$ and *mer*-$[Ru(Li)_3]^{2+}$ ($i=2$, 3)[5] with four singlets of equal intensities for the methyl groups Me$^1$. For the $C_3$-symmetrical *fac*-$[Ru(Li)_3]^{2+}$ ($i=2$, 3), the three ligands are equivalent and Me$^1$ appears as a singlet at $\delta=2.25$ ppm (*fac*-$[Ru(L2)_3]^{2+}$ Figure 2a) or at $\delta=2.23$ ppm (*fac*-$[Ru(L3)_3]^{2+}$ (Figure 2b). The three other signals of equal intensities are assigned to Me$^1$ in the $C_1$-symmetrical *mer*-$[Ru(Li)_3]^{2+}$ ($i=2$, 3), in which each ligand is nonequivalent (Figure 1). A complete and reliable assignment (Table S1, Supporting Information) has been performed: 1) by using two-dimensional $^1$H–$^1$H COSY and $^1$H–$^1$H NOESY spectra and 2) by comparison with the $^1$H NMR spectra of the pure isomers **1–3** (Figure 3a–c, respectively). The statistical 1:3 *fac*/*mer* mixtures found for $[Ru(L2)_3](ClO_4)_2\cdot 2H_2O$ and $[Ru(L3)_3](ClO_4)_2\cdot CH_3CN\cdot H_2O$ match the 0.33 ratio reported for the analogous complex $[Ru(L6)_3](PF_6)_2$,[5b] although deviations favoring the meridional isomer are often observed because of steric constraints in the facial one.[5,17]

$[Ru(L2)_3](ClO_4)_2\cdot 2H_2O$ was dissolved in dichloromethane, extracted with an aqueous 0.1 mol L$^{-1}$ solution of $Na_2Sb_2[(+)\text{-}C_4O_6H_2]_2\cdot 5H_2O$,[4a] and sorbed onto a Sephadex SP-C25 ion exchange resin. Further elution with $Na_2Sb_2[(+)\text{-}C_4O_6H_2]_2\cdot 5H_2O$ (0.1 mol L$^{-1}$ in water) provided two successive red bands which were collected separately. Red solids were finally isolated by precipitation with $NaClO_4$. Their elemental analyses match the original empirical formula $[Ru(L2)_3](ClO_4)_2\cdot 2H_2O$, but the $^1$H NMR spectrum of fraction **I** (with the shortest retention time: **1**, yield = 69 %) shows only the three nonequivalent bidentate ligands of the $C_1$-symmetrical *mer*-$[Ru(L2)_3]^{2+}$ (Figure 3a).[5,17] Clearly, fraction **II** (with the longest retention time: **2**, yield = 20 %) exhibits a much simpler $^1$H NMR spectrum corresponding to the $C_3$-symmetrical *fac*-$[Ru(L2)_3]^{2+}$ (Figure 3b). The satisfying 89 % recovery of the original compound and the approximate invariance of the *fac/mer* ratio (0.29:1 after chromatography) demonstrate that $[Ru(L2)_3]^{2+}$ is inert enough in a polar solvent to be separated by chromatogaphy (3–4 h time scale). However, when $[Ru(L3)_3](ClO_4)_2\cdot CH_3CN\cdot H_2O$ was subjected to chromatography under the same conditions, a single large red band was collected. Precipitation with $NaClO_4$ gave a red microcrystalline precipitate displaying the same constitution

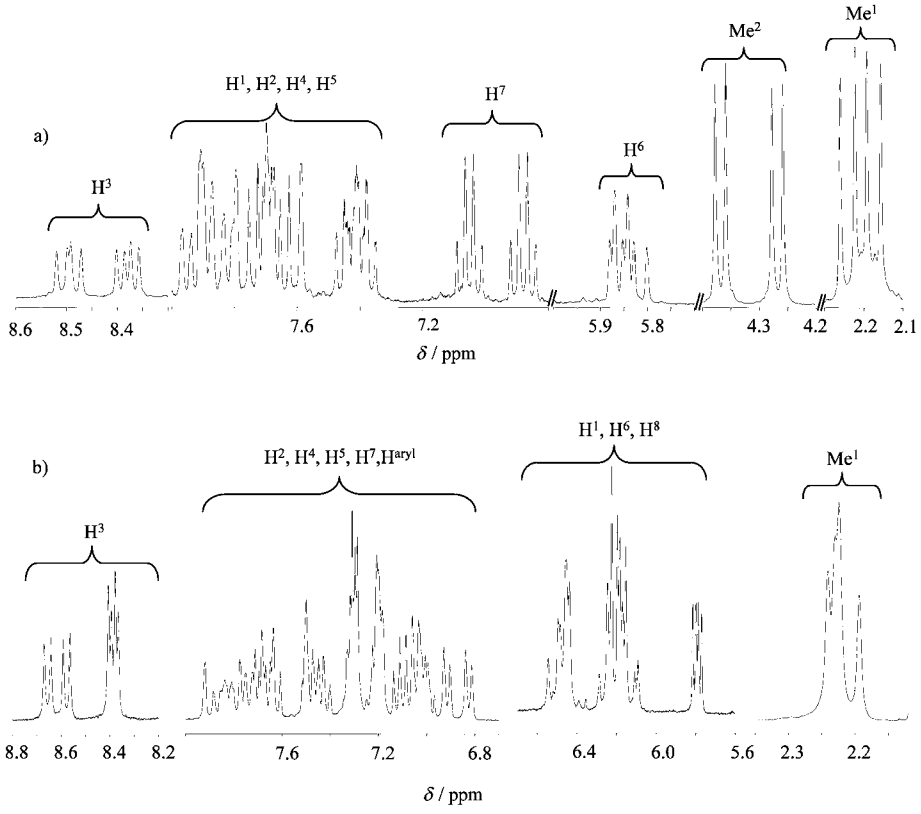


Figure 2. $^1$H NMR spectra of a) $[Ru(L2)_3](ClO_4)_2\cdot 2H_2O$ and b) $[Ru(L3)_3](ClO_4)_2\cdot CH_3CN\cdot H_2O$, highlighting the 1:3 mixture of *fac*/*mer* isomers ($CD_3CN$, 298 K; numbering as in Figure 1).

 © 2004 Wiley-VCH Verlag GmbH & Co. KGaA, Weinheim 

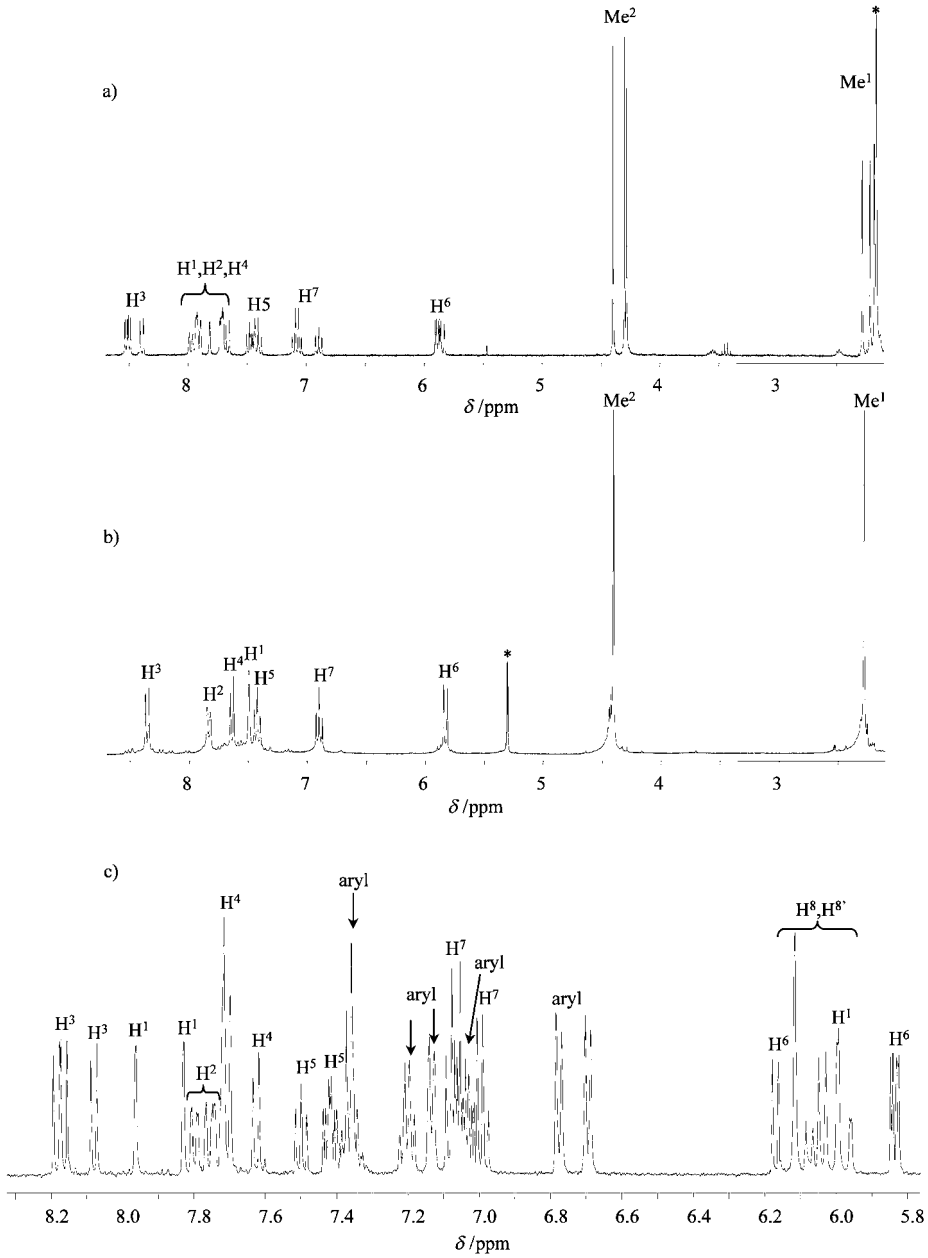


Figure 3. $^1$H NMR spectra of a) *mer*-$[Ru(L2)_3](ClO_4)_2\cdot 2H_2O$ (**1**), b) *fac*-$[Ru(L2)_3](ClO_4)_2\cdot 2H_2O$ (**2**) and c) *mer*-$[Ru(L3)_3](ClO_4)_2\cdot CH_3CN\cdot H_2O$ (**3**) ($CD_3CN$, 298 K; * denotes residual peak of solvent; numbering as in Figure 1 and Scheme 1).

as the original complex (**3**, yield = 90%). However, its $^1$H NMR spectrum corresponds to the exclusive existence of *mer*-$[Ru(L3)_3]^{2+}$ in solution (Figure 3c), which suggests that 1) a relatively fast *fac*-$[Ru(L3)_3]^{2+} \rightleftharpoons$ *mer*-$[Ru(L3)_3]^{2+}$ isomerisation process occurs during the chromatographic separation and 2) *mer*-$[Ru(L3)_3]^{2+}$ is stabilised beyond the expected statistical entropic contribution: $\Delta G_1^{stat} = -T\Delta S_1^{stat} = -2.7\ kJ\,mol^{-1}$ at 298 K and $K_1^{stat} = 3$.[5a,18] According to the limit of detection of *fac*-$[Ru(L3)_3]^{2+}$ by $^1$H NMR spectroscopy ($\geq 1\%$), we calculate from the above equilibrium that $K_1([Ru(L3)_3]^{2+}) \geq 99$, and $\Delta G^{\ominus}_{isomerization}([Ru(L3)_3]^{2+}) \leq -11.4\ kJ\,mol^{-1}$.

**Kinetics of the *fac*-$[Ru(Li)_3]^{2+} \rightleftharpoons$ *mer*-$[Ru(Li)_3]^{2+}$ ($i$ = 2, 3) iomerisation process in solution**: In weakly polar $CD_2Cl_2$ ($\varepsilon_{rel} = 8.9$), the original 1:3 mixture of *fac*-$[Ru(L2)_3]^{2+}$ and *mer*-$[Ru(L2)_3]^{2+}$ remains invariant for months. In ethanol ($\varepsilon_{rel} = 24.5$), small changes occur after one week, and in more polar solvents ($CD_3CN$, $\varepsilon_{rel} = 37.5$; $CD_3OD$, $\varepsilon_{rel} = 32.7$) the signals corresponding to the facial isomer disappear slowly within five days to give *mer*-$[Ru(L2)_3]^{2+}$ exclusively according to Equation (1) (Figure 4).

$$fac\text{-}[Ru(Li)_3]^{2+} \underset{k_{mer}}{\overset{k_{fac}}{\rightleftharpoons}} mer\text{-}[Ru(Li)_3]^{2+} \quad K_1 = \frac{k_{fac}}{k_{mer}} \tag{1}$$

The complete mathematical treatment of the time-dependent concentrations of *fac*-$[Ru(L2)_3]^{2+}$ ($|fac(t)|$)and of *mer*-$[Ru(L2)_3]^{2+}$ ($|mer(t)|$) according to Equation (1) with


© 2004 Wiley-VCH Verlag GmbH & Co. KGaA, Weinheim

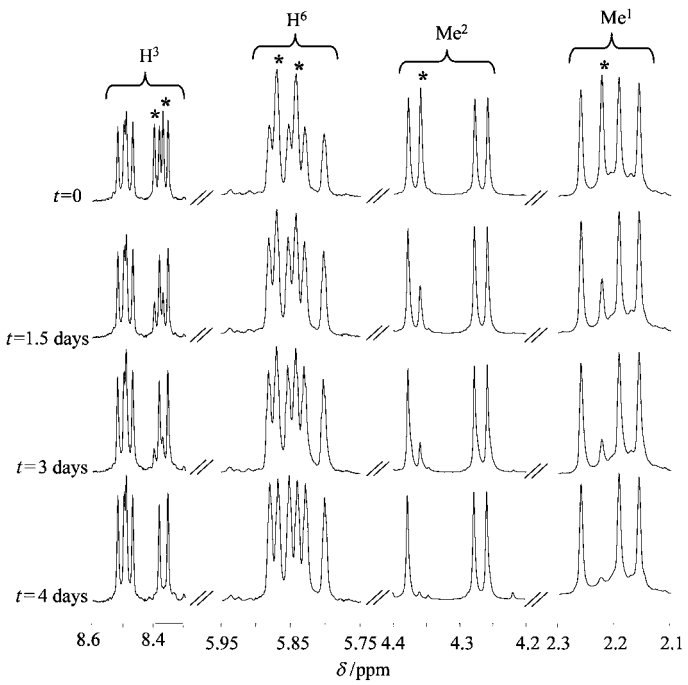


Figure 4. Selected parts of the time-dependent $^1$H NMR spectra recorded for $[Ru(L2)_3](ClO_4)_2 \cdot 2H_2O$, showing the slow isomerisation of *fac*-$[Ru(L2)_3]^{2+}$ (marked *) into *mer*-$[Ru(L2)_3]^{2+}$ according to Equation (1) ($CD_3CN$, 298 K; numbering as in Figure 1).

the first-order kinetic constants $k_{fac}$ and $k_{mer}$ leads to Equations (2) and (3).[19]

$$|fac(t)| = \frac{k_{mer}}{k_{fac}+k_{mer}}(|fac(0)|+|mer(0)|)+ \left(\frac{k_{fac}|fac(0)|-k_{mer}|mer(0)|}{k_{fac}+k_{mer}}\right)\exp(-(k_{fac}+k_{mer})t) \quad (2)$$

$$|mer(t)| = \frac{k_{fac}}{k_{fac}+k_{mer}}(|fac(0)|+|mer(0)|)- \left(\frac{k_{fac}|fac(0)|-k_{mer}|mer(0)|}{k_{fac}+k_{mer}}\right)\exp(-(k_{fac}+k_{mer})t) \quad (3)$$

As previously noticed for $[Ru(L3)_3]^{2+}$, *mer*-$[Ru(L2)_3]^{2+}$ is the only isomer detected at the thermodynamic equilibrium in $CD_3CN$ or $CD_3OD$, which implies that the latter complex is stabilised beyond the statistical entropic contribution for which we expect a final 1:3 mixture of *fac* and *mer* isomers ($\Delta S_1^{stat} = 9.1\ J\,mol^{-1}\,K^{-1}$, $\Delta H_1^{stat} = 0\ kJ\,mol^{-1}$, $\Delta G_1^{stat} = T\Delta S_1^{stat} = -2.7\ kJ\,mol^{-1}$ at 298 K and $K_1^{stat} = 3$).[5a,18] Again, if we fix the limit of detection of *fac*-$[Ru(L2)_3]^{2+}$ by $^1$H NMR spectroscopy at around 1%, we calculate from Equation (1) that $K_1([Ru(L2)_3]^{2+}) \geq 99$ and $\Delta G^{\ominus}_{isomerisation}([Ru(L2)_3]^{2+}) \leq -11.4\ kJ\,mol^{-1}$. This translates into $k_{fac} \geq 99\,k_{mer}$ for $[Ru(L2)_3]^{2+}$ in $CD_3CN$ at 298 K, which allows us to neglect the latter constant and Equations (2) and (3) reduce to the classical Equations (4) and (5).

$$|fac(t)| = |fac(0)|\exp(-k_{fac}t) \quad (4)$$

$$|mer(t)| = |mer(0)| - |fac(0)|\exp(-k_{fac}t) \quad (5)$$

The plot of ($|fac(t)|$) versus $t$ for *fac*-$[Ru(L2)_3]^{2+}$ in $CD_3CN$ (298 K) is indeed linear and its slope corresponds to $-k_{fac}$ (Figure S1a, Supporting Information), from which we calculate $k_{fac}^{298}([Ru(L2)_3]^{2+}) = 4.7(6)\times10^{-6}\ s^{-1}$ with a half-life of $\tau_{1/2}^{298}([Ru(L2)_3]^{2+}) = 41.03$ h, in agreement with the limited isomerisation observed during the chromatographic separation of $[Ru(L2)_3]^{2+}$. However, the slow formation of monocrystals of $[Ru(L2)_3](ClO_4)_2$ resulting from diffusion of heavy ethers (*tert*-butyl methyl ether or diisopropyl ether) into a solution of the complex in acetonitrile is limited to the isolation of *mer*-$[Ru(L2)_3](ClO_4)_2$. Interestingly, the introduction of the bulky benzyl substituents in $[Ru(L3)_3]^{2+}$ significantly increases the lability of the *fac*→*mer* isomerisation process, and the analysis of the linear plot $\ln(|fac(t)|)$ versus $t$ (Figure S1b, Supporting Information) gives $k_{fac}^{298}([Ru(L3)_3]^{2+}) = 1.3(1)\times10^{-4}\ s^{-1}$ with a half-life of $\tau_{1/2}^{298}([Ru(L3)_3]^{2+}) = 1.45$ h. This 28-fold increase in velocity explains the exclusive isolation of *mer*-$[Ru(L3)_3](ClO_4)_2$ after column chromatography. We obtained monocrystals of both *mer*-$[Ru(Li)_3](ClO_4)_2$ ($i$=2, 3), but the X-ray diffraction data show that the benzimidazole and the pyridine rings in *mer*-$[Ru(L2)_3](ClO_4)_2$ are so similar that they crystallise randomly over two positions. This limitation is removed for *mer*-$[Ru(L3)_3](ClO_4)_2$ (**4**) because the benzyl groups connected to the benzimidazole rings induce greater structural differences between the two aromatic rings, and a regular packing results in the crystals of **4**. In the absence of detailed variable-temperature thermodynamic and kinetic studies [that is, separation of the enthalpic and entropic contributions to the thermodynamic (van't Hoff equation) and to the kinetic (Eyring equation) properties], the origins of the increased lability of *fac*-$[Ru(Li)_3]^{2+}$ observed 1) on going from $[Ru(L2)_3]^{2+}$ to $[Ru(L3)_3]^{2+}$ and 2) on increasing the polarity of the solvent remain difficult to rationalise. However, this observation has important synthetic consequences for the use of $Ru^{II}$ as a "labile" partner in strict self-assembly processes with L1, because the required "error checking" processes become available on the timescale of an hour under judiciously chosen conditions.[10]

**Crystal and molecular structure of *mer*-$[Ru(L3)_3](ClO_4)_2$ (4)**: The crystal structure of **4** shows $Ru^{II}$ in a six-coordinate environment, coordinated by the nitrogen donor atoms of the three bidentate benzimidazol-2-ylpyridine ligands. Ligands a and b adopt the same orientation, while ligand c is reversed; this confirms the formation of the cation *mer*-$[Ru(L3)_3]^{2+}$ (Figure 5). One ionic perchlorate is disordered (see Experimental Section), but shows no other interesting feature. The coordination sphere of $Ru^{II}$ can best be described as an octahedron flattened along a pseudo-$C_3$ axis defined by the least-squares line passing through the ruthenium and the barycentres of the triangular faces $F_1$ (N1a,N1b,N3c) and $F_2$ (N1c,N3a,N3b; Figure 5).

The classical geometrical analysis that measures the bending ($\phi$), flattening ($\theta_i$) and twist ($\omega_{ij}$) of the octahedron[8,9,20] displays a negligible bending ($\phi = 177.4°$ compared with $\phi = 180°$ for a perfect octahedron; Table S2, Supporting Information), but a significant flattening along the pseudo-$C_3$ axis

 © 2004 Wiley-VCH Verlag GmbH & Co. KGaA, Weinheim 

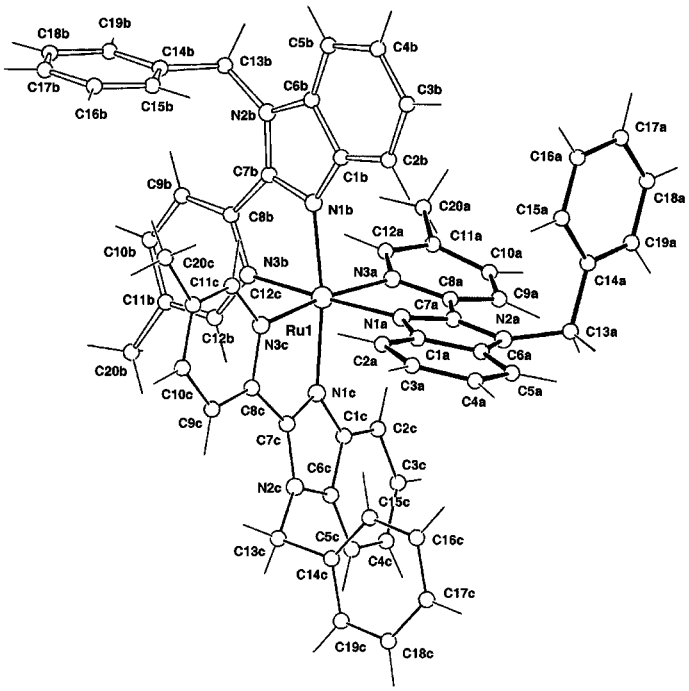


Figure 5. Perspective view of *mer*-$[Ru(L3)_3]^{2+}$ in the crystal structure of **4** showing the atomic numbering scheme.

($\theta_i = 57.6$–$62.8°$, average 60.3(1.8)° compared with $\theta_i = 54.7°$ for a perfect octahedron; Table S2, Supporting Information). This distortion is typical for the [M(benzimidazol-2-ylpyridine)$_3$] units in the heterobimetallic d–f helicates $[MLn(L1)_3]^{n+}$ (M = $Fe^{II}$,[21] $Cr^{III}$,[9] $Co^{III}$[8]), and it results from the constrained intraligand bite angles, which are smaller (77.1–77.7°, average 77.4(3)° Table 1), than the 90° required for a perfect octahedron. The twist of the two triangular faces $F_1$ and $F_2$ in *mer*-$[Ru(L3)_3]^{2+}$ ($\omega_{ij}$ intraligand = 50.6–53.6, average 51.9(1.5)°; Table S2, Supporting Information) corresponds to a slight distortion from a perfect octahedron ($\omega_{ij}$ intraligand = 60°) towards a trigonal prism ($\omega_{ij}$ intraligand = 0°) as previously noticed in the crystal structure of $[FeLa(L1)_3]^{5+}$.[21] The same geometrical analysis has been applied to the reference complex [Ru(2,2′-bipyridine)$_3$]$(ClO_4)_2$[22] and shows very similar distortions (average angles: $\phi = 177.4°$, $\theta_i = 59.1(1.4)°$, $\omega_{ij}$ intraligand = 51.0(7)°; Table S2, Supporting Information). Similarly, the Ru–N1(benzimidazole) bonds (average: 2.06(1) Å; Table 1) and Ru–N3(pyridine) bonds (average: 2.078(2) Å; Table 1) in *mer*-$[Ru(L3)_3]^{2+}$ closely match Ru–N(pyridine) = 2.058(2) Å reported for [Ru(2,2′-bipyridine)$_3$]$(ClO_4)_2$.[22]

We thus conclude that the replacement of a six-membered pyridine ring in 2,2′-bipyridine with a five-membered imidazole ring in L3 has a negligible effect on the arrangement of the three bidentate ligands around $Ru^{II}$, and that the significantly increased lability of the *fac*-$[Ru(L3)_3]^{2+} \rightleftharpoons$ *mer*-$[Ru(L3)_3]^{2+}$ isomerisation cannot be ascribed to a specific electronic and/or steric effect induced by the benzyl substituents that affects the Ru–N bonds. Although they are not relevant to the solution behaviour, it is worth noting that intermolecular π-stacking interactions occur between the pyridine ring of ligand c and the peripheral phenyl ring of the benzyl substituent of ligand a (interplanar angle 5.86(3)°, average interplanar distance 3.49 Å; Figure S2, Supporting Information).

**Electrochemical and photophysical properties of 1–3**: The cyclic voltammograms of *mer*-$[Ru(L2)_3]^{2+}$ and *fac*-$[Ru(L2)_3]^{2+}$ in acetonitrile (0.1 mol $L^{-1}$ $[N(nBu)_4]ClO_4$) are identical within experimental error and show the expected reversible oxidation wave assigned to the metal-centred $Ru^{II}/Ru^{III}$ process ($E_{1/2}([Ru(L2)_3]^{3+}/[Ru(L2)_3]^{2+}) = 0.94$ V versus SCE; Table 2), together with the three ligand-centred reductions in the range −1.37 to −1.82 V versus SCE (Table 2; Figure 6).

This behaviour parallels that reported for [Ru(2,2′-bipyridine)$_3$]$^{2+}$[13,23] except that the $Ru^{II}/Ru^{III}$ process in $[Ru(L2)_3]^{2+}$ is cathodically shifted by 330 mV, and the first ligand reduction is almost invariant (cathodic shift 60 mV; Table 2). Since the latter process reflects the energy of the $\pi^*$-accepting orbitals in the complex,[24] we deduce that L2 and 2,2′-bipyridine display comparable π-accepting properties. The destabilisation of the electron-rich $Ru^{II}$ in $[Ru(L2)_3]^{2+}$ thus results from L2 being a stronger π-donor than 2,2′-bipyridine in the tris-chelate–ruthenium complexes, and this is strongly supported by the 4130–4790 $cm^{-1}$ red shift of the ligand-centred $\pi \rightarrow \pi^*$ transitions measured for $[Ru(Li)_3]^{2+}$ in so-

Table 1. Selected bond lengths [Å] and bond angles [°] in *mer*-$[Ru(L3)_3](ClO_4)_2$ (**4**) and [Ru(2,2′-bipyridine)$_3$]$(ClO_4)_2$.

| | *mer*-$[Ru(L3)_3](ClO_4)_2$ (**4**) | | | [Ru(2,2′-bipyridine)$_3$]$(ClO_4)_2$[a] | | |
|---|---|---|---|---|---|---|
| | ligand a | ligand b | ligand c | | ligands a,b | ligand c |
| Ru–N1 | 2.073(3) | 2.054(3) | 2.068(3) | Ru–N1 | 2.059(3) | 2.056(3) |
| Ru–N3 | 2.079(3) | 2.076(3) | 2.069(3) | Ru–N11 | 2.060(3) | 2.056(3) |
| N1-Ru-N3 | 77.3(1) | 77.7(1) | 77.1(1) | N1-Ru-N11 | 78.6(1) | 78.5(1) |
| N1a-Ru-N1b | 101.7(1) | | | N1-Ru-N11 | 97.9(1) | |
| N1a-Ru-N1c | 85.0(1) | | | N1-Ru-N11′ | 92.0(1) | |
| N1a-Ru-N3c | 95.5(1) | | | $N1^A$-Ru-N11′ | 94.9(1) | |
| N1b-Ru-N3a | 88.6(1) | | | N11-Ru-$N11'^A$ | 94.8(1) | |
| N1b-Ru-N3c | 96.8(1) | | | | | |
| N1c-Ru-N3a | 98.1(1) | | | | | |
| N1c-Ru-N3b | 96.1(1) | | | | | |
| N3a-Ru-N3b | 97.0(1) | | | | | |
| N3b-Ru-N3c | 90.3(1) | | | | | |
| N1b-Ru-N1c | 171.4(1) | | | N1-Ru-$N11^A$ | 172.6(1) | |
| N1a-Ru-N3b | 174.3(1) | | | N11′-Ru-N·$N11'^A$ | 171.0(1) | |
| N3a-Ru-N3c | 171.7(1) | | | | | |

[a] Taken from ref. [22]. [Ru(2,2′-bipyridine)$_3$]$(ClO_4)_2$ possesses a crystallographic twofold axis, and ligands a and b are thus equivalent and related by the symmetry operation A = $-x, y, 0.5-z$.


© 2004 Wiley-VCH Verlag GmbH & Co. KGaA, Weinheim

Table 2. Electrochemical properties of *mer*-$[Ru(L2)_3](ClO_4)_2$ (**1**), *fac*-$[Ru(L2)_3](ClO_4)_2$ (**2**) and *mer*-$[Ru(L3)_3](ClO_4)_2$ (**3**) in $CH_3CN$ + 0.1 mol $L^{-1}$ $[N(nBu)_4]ClO_4$ (298 K).[a]

| | $E_{1/2}$ ($Ru^{III}/Ru^{II}$) | $E_{1/2}$ ($[RuL_3]^{2+}/[RuL_3]^{+}$) | $E_{1/2}$ ($[RuL_3]^{+}/[RuL_3]$) | $E_{1/2}$/ ($[RuL_3]/[RuL_3]^{-}$) | Ref. |
|---|---|---|---|---|---|
| **1** | 0.94 | −1.37 | −1.56 | −1.82 | this work |
| **2** | 0.94 | −1.37 | −1.56 | −1.82 | this work |
| **3** | 1.08 | −0.96[b] | −1.26[b] | −1.41[b] | this work |
| $[Ru(2,2'\text{-bipy})_3]^{2+}$ | 1.27 | −1.31 | −1.50 | −1.77 | [13] |
| $[Ru(L5)_3]^{2+}$ | 0.61 | –[c] | –[c] | –[c] | [25] |
| $[Ru(L6)_3]^{2+}$ | 0.59 | −2.00 | −2.20 | – | [25] |

[a] Half-wave potentials $E_{1/2}$ [V], versus SCE. [b] Irreversible redox processes; $E_{1/2}$ for the cathodic process is reported. [c] No observed reduction wave (ref. [25]).

lution ($i=2$, 3; $10^{-4}$ mol $L^{-1}$ in ethanol/methanol (4:1); Table 3). This trend parallels that reported for the analogous homoleptic complexes $[Ru(L5)_3]^{2+}$ ($E_{1/2}([Ru(L5)_3]^{3+}/[Ru(L5)_3]^{2+}) = 0.61$ V versus SCE),[25] $[Ru(L6)_3]^{2+}$ ($E_{1/2}([Ru(L6)_3]^{3+}/[Ru(L6)_3]^{2+}) = 0.59$ V versus SCE),[25] and for the heteroleptic complex $[Ru(2,2'\text{-bipyridine})_2(L4)]^{2+}$ ($E_{1/2}([Ru(bipy)_2(L4)]^{3+}/[Ru(bipy)_2(L4)]^{2+} = 1.18$ V versus SCE).[26] The introduction of benzyl substituents in *mer*-$[Ru(L3)_3]^{2+}$ induces a global anodic shift of 140–410 mV affecting all redox processes (Table 2), but the main difference concerns the irreversibility of the ligand-centred reduction processes (Figure 6). However, the difference $\Delta E_{1/2}$ between the oxidation and the first reduction process for $[Ru(L2)_3]^{2+}$ ($\Delta E_{1/2} = E_{1/2}([Ru(L2)_3]^{3+}/[Ru(L2)_3]^{2+}) - E_{1/2}([Ru(L2)_3]^{2+}/[Ru(L2)_3]^{+}) = 2.31$ V) and *mer*-$[Ru(L3)_3]^{2+}$ ($\Delta E_{1/2} = 2.04$ V)

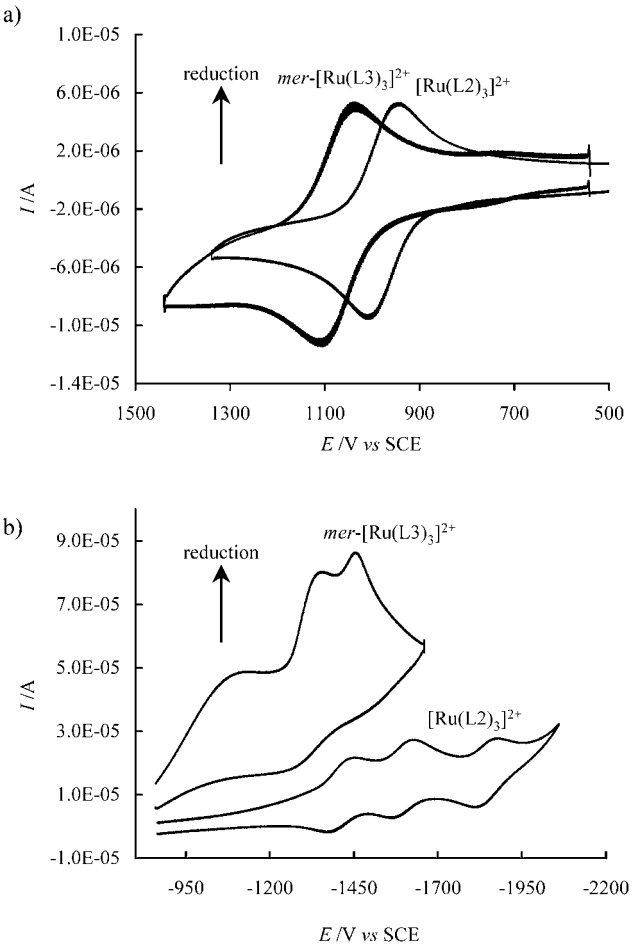


Figure 6. Cyclic voltammograms of $[Ru(L2)_3]^{2+}$ and *mer*-$[Ru(L3)_3]^{2+}$ for a) oxidation and b) reduction processes ($CH_3CN$ + 0.1 mol $L^{-1}$ $[N(nBu)_4]ClO_4$, 100 mV $s^{-1}$, 298 K).

Table 3. Photophysical properties of *mer*-$[Ru(L2)_3](ClO_4)_2$ (**1**), *fac*-$[Ru(L2)_3](ClO_4)_2$ (**2**), *mer*-$[Ru(L3)_3](ClO_4)_2$ (**3**) and *HHH*-$[RuLu(L1)_3](CF_3SO_3)_5$ (**5**) in ethanol/methanol (4:1; $10^{-4}$ mol $L^{-1}$).

| | $T$ [K] | $\pi\rightarrow\pi^*$(abs) [$cm^{-1}$][a] | $^1$MLCT(abs) [$cm^{-1}$][a] | $^3$MLCT(em) [$cm^{-1}$][b] | $\tau$(em) [$\mu s^{-1}$] | $\Phi$(em) |
|---|---|---|---|---|---|---|
| **1** | 296 | 30770 (41250) | 21370 (10730) | 14325 | 0.074(8) | 0.0010(1) |
| | 77 | – | – | 15150 | 1.62(3) | 0.041(4) |
| **2** | 296 | 30960 (39850) | 21185 (8440) | 14345 | 0.050(5) | 0.0010(1) |
| | 77 | – | – | 15950 | 3.2(1) | 0.052(5) |
| **3** | 296 | 30300 (41300) | 21320 (11570) | 14450 | 0.112(4) | 0.0030(3) |
| | 77 | – | – | 15220 | 1.70(6) | 0.039(4) |
| $[Ru(2,2'\text{-bipy})_3]^{2+}$ | 296 | 35090 (70000) | 22170 (14730) | 16285 | 0.643(4) | 0.055(6) |
| $[Ru(2,2'\text{-bipy})_3]^{2+}$ | 77 | – | – | 17210 | 5.2(2) | 0.36(4) |
| **5** | 296 | 39840 (22120) 29850 (55000) | 21100 (11350) | 14730 | 0.242(5) | 0.0056(6) |
| [c] | 296 | 39525 (22050) 29940 (55000) | 21100 (11100) | 14730 | 0.384(6) | 0.010(1) |
| | 77 | – | – | 15470 | 2.0(1) | 0.028(3) |

[a] Molar extinction coefficients are given between parentheses. [b] $\nu_{exc} = 20492$ $cm^{-1}$ and the values reported at 77 K corrrespond to the 0–0 phonon transitions. [c] In acetonitrile.

remain significantly smaller than $\Delta E_{1/2} = 2.58$ V calculated for $[Ru(2,2'\text{-bipyridine})_3]^{2+}$ in the same conditions.[13] We therefore expect that the $^1$MLCT and $^3$MLCT excited states are located at lower energies in $[Ru(Li)_3]^{2+}$ ($i=2$, 3) than in $[Ru(2,2'\text{-bipyridine})_3]^{2+}$, assuming that the net reorganisational free energy contribution $\chi_r$ is similar in these complexes.[1d,27] The absorption spectra recorded in solution ($10^{-4}$ mol $L^{-1}$ in ethanol/methanol (4:1)) indeed confirms a 800–1000 $cm^{-1}$ red shift of the $^1$MLCT transition on going from $[Ru(2,2'\text{-bipyridine})_3]^{2+}$ ($\nu = 22170$ $cm^{-1}$) to $[Ru(Li)_3]^{2+}$ ($i=2$, 3; $21185 \le \nu \le 21370$ $cm^{-1}$; Table 3, Figure 7a). *mer*-$[Ru(L2)_3]^{2+}$ and *fac*-$[Ru(L2)_3]^{2+}$ display slightly dif-

 © 2004 Wiley-VCH Verlag GmbH & Co. KGaA, Weinheim 

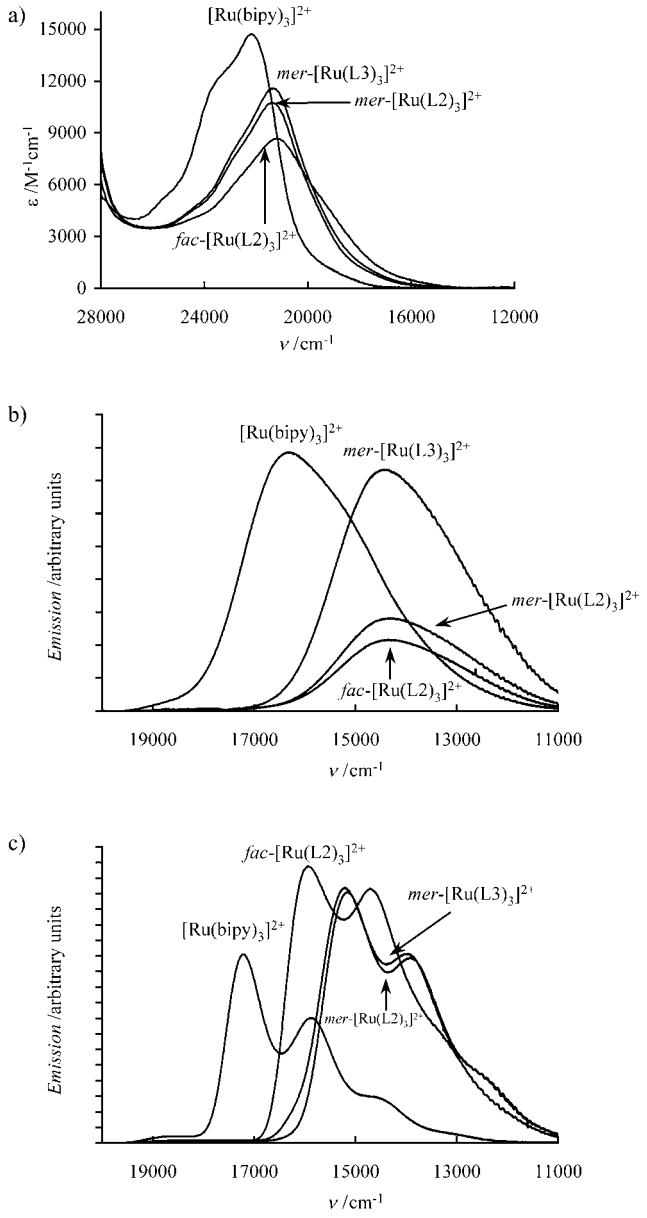


Figure 7. a) Absorption spectra of $[Ru(Li)_3]^{2+}$ ($i=2$, 3) and [Ru(2,2′-bipyridine)$_3$]$^{2+}$ in ethanol/methanol (4:1, 296 K) showing the $^1$MLCT transition. b) Emission spectra of $[Ru(Li)_3]^{2+}$ ($i=2$, 3; $10^{-4}$ mol L$^{-1}$) and [Ru(2,2′-bipyridine)$_3$]$^{2+}$ ($10^{-5}$ mol L$^{-1}$) in ethanol/methanol (4:1) at 296 K and c) in frozen glasses at 77 K.

ferent absorption spectra and spectroscopic properties, as previously reported for analogous [Ru(pyridine-azole)$_3$]$^{2+}$ complexes.[6a]

On the basis of the pioneering work of Lever and co-workers,[28] Endicott and co-workers[27] proposed a useful and simple approximate correlation between $\Delta E_{1/2}$ and the spectroscopic energy of the $^1$MLCT transition in Ru$^{II}$ complexes: $h\nu_{max}(abs) = F\Delta E_{1/2} + \chi_r$ in which $F$ stands for the Faraday constant and $\chi_r$ corresponds to the reorganisational free energy. Taking $\nu_{max}$(abs) at room temperature from Table 3 and $\Delta E_{1/2}$ reported above, we calculate that $\chi_r$ increases in the order $\chi_r([Ru(2,2'\text{-bipyridine})_3]^{2+}) = 1360\ cm^{-1} \ll \chi_r(fac\text{-}[Ru(L2)_3]^{2+}) = 2550\ cm^{-1} \approx \chi_r(mer\text{-}[Ru(L2)_3]^{2+}) = 2740\ cm^{-1} < \chi_r(mer\text{-}[Ru(L3)_3]^{2+}) = 4870\ cm^{-1}$. The last value is not very reliable because of the irreversibility of the corresponding reduction wave. The higher reorganisational free energies exhibited by $[Ru(Li)_3]^{2+}$ ($i=2$, 3) partially overcome the considerably higher value of $\Delta E_{1/2}$ characterizing [Ru(2,2′-bipyridine)$_3$]$^{2+}$, and this may explain the only minor global red shift of the $^1$MLCT transition observed on going from [Ru(2,2′-bipyridine)$_3$]$^{2+}$ to $[Ru(Li)_3]^{2+}$ ($i=2$, 3; Figure 7a). The emission spectra of [Ru(2,2′-bipyridine)$_3$]$^{2+}$ and $[Ru(Li)_3]^{2+}$ ($i=2$, 3) obtained upon excitation of the $^1$MLCT state originate from the $^3$MLCT state[1] and confirm the red shift induced in these last complexes (Figure 7b,c). The lifetimes $\tau$($^3$MLCT) and the associated quantum yields $\Phi$ measured at low temperature in frozen glasses (77 K) are significantly reduced on going from [Ru(2,2′-bipyridine)$_3$]$^{2+}$ to $[Ru(Li)_3]^{2+}$ ($i=2$, 3; Table 3). That this reduction is even greater at room temperature is diagnostic for the existence of thermally activated de-excitation pathways involving d–d excited states close in energy.[1,2] For [Ru(2,2′-bipyridine)$_3$]$^{2+}$, the zero-point energy difference between the d–d and the $^3$MLCT state, $\Delta E^{\ominus} = E^{\ominus}$(d–d)$-E^{\ominus}$($^3$MLCT), has been estimated to be around 4040 cm$^{-1}$.[29] From the maximum of the emission band, $\nu_{max}$(em), the zero-point energy of the $^3$MLCT state can be calculated according to $E^{\ominus}(^3MLCT) = h\nu_{max}(em) + \chi_r$. Therefore the actual zero-point energy of the d–d state is given by $E^{\ominus}$(d–d)$= h\nu_{max}(em) + \chi_r + \Delta E^{\ominus}$. From the room temperature emission spectrum shown in Figure 7b, and assuming the reorganisational energy of the ground state to be the same as that in the MLCT states, $E^{\ominus}$(d–d)$\approx$22 500 cm$^{-1}$ for [Ru(2,2′-bipyridine)$_3$]$^{2+}$. Since the ratio of Jørgensen's ligand-field parameters[30] between the bipyridine and benzimidazole-2-ylpyridine units amounts to $f_{benzimidazol\text{-}2\text{-}ylpyridine}/f_{bipyridine} = 0.87$,[31] we deduce that the ratio of the ligand-field splittings is $10Dq([Ru(Li)_3]^{2+})/10Dq([Ru(2,2'\text{-bipyridine})_3]^{2+}) = 0.87$. Even though $10Dq$ for a given ligand depends upon the metal–ligand distance, this ratio is not only valid at the equilibrium geometry of the ground state, but also for other geometries, and therefore $E^{\ominus}$(d–d)$\approx$19 500 cm$^{-1}$ for $[Ru(Li)_3]^{2+}$ ($i=2$, 3). This, in turn, translates into $\Delta E^{\ominus} = E^{\ominus}$(d–d)$-h\nu_{max}(em) - \chi_r \approx 19500 - 14370 - 2650 \approx 2500\ cm^{-1}$ for *mer*/*fac*-[Ru(L2)$_3$]$^{2+}$, which is indeed lower than that found in [Ru(2,2′-bipyridine)$_3$]$^{2+}$ (4040 cm$^{-1}$),[29] in line with the shorter lifetimes and the quantum yields, which are found to be one order of magnitude smaller for [Ru(L2)$_3$]$^{2+}$ at 296 K (Table 3). The rather uncertain value of $\chi_r$ for [Ru(L3)$_3$]$^{2+}$ due to the irreversibility of the reduction wave in the cyclic voltammogram excludes the possibility of a reliable estimate of $\Delta E^{\ominus}$ for this complex, but from the quantum yields and luminescence lifetimes at both 77 and 298 K we conclude that it must be of the same magnitude as that for [Ru(L2)$_3$]$^{2+}$.

**Use of the "labile" *fac*-[Ru(benzimidazol-2-ylpyridine)$_3$]$^{2+}$ $\rightleftharpoons$*mer*-[Ru(benzimidazol-2-ylpyridine)$_3$]$^{2+}$ isomerisation process in solution for the strict self-assembly of [RuLu(L1)$_3$]$^{5+}$**: Preliminary attempts to make L1 react with [Ru(dmso)$_4$Cl$_2$] or [Ru(dmso)$_5$(H$_2$O)](CF$_3$SO$_3$)$_2$·H$_2$O in eth-


© 2004 Wiley-VCH Verlag GmbH & Co. KGaA, Weinheim

anol produced intricate mixtures of *mer*-$[Ru(L1)_3]^{2+}$ and *fac*-$[Ru(L1)_3]^{2+}$, in which $Ru^{II}$ was coordinated by the three bidentate segments, together with considerable quantities of noncharacterised species involving the complexation of the tridentate segments. Taking advantage of the relative lability of $[Ru(benzimidazol\text{-}2\text{-}ylpyridine)_3]^{2+}$ in polar solvents, we performed the same reaction by using L1 (3 equiv) with an equimolar mixture of $[Ru(dmso)_5(H_2O)](CF_3SO_3)_2\cdot H_2O$ (1 equiv) and $Lu(CF_3SO_3)_3\cdot 1.4\,H_2O$ in hot ethanol. Since only *fac*-$[Ru(L1)_3]^{2+}$ can coordinate $Lu^{III}$ efficiently by wrapping the three tridentate benzimidazole–pyridine–carboxamide units to give the triple-stranded helicate *HHH*-$[RuLu(L1)_3]^{5+}$ (where *HHH* stands for head-to-head-to-head),[10c] the facial conformation is strongly stabilised by enthalpic and entropic contributions,[8–10] and we have indeed isolated *HHH*-$[RuLu(L1)_3](CF_3SO_3)_5\cdot 2\,CH_3OH\cdot H_2O$ (**5**) in 70% yield after recrystallisation. The $^1H$ NMR spectrum confirms the exclusive formation of the $C_3$-symmetrical *HHH*-$[RuLu(L1)_3]^{5+}$ in solution, resulting from three ligands adopting a parallel arrangement (Figure 8). The 23 observed $^1H$ NMR signals correspond to protons connected to 20 carbon atoms for which $H^7$–$H^8$, $H^{15}$–$H^{16}$ and $H^{17}$–$H^{18}$ are diastereotopic as a result of the blocked $P\rightleftharpoons M$ helical interconversion occurring in *HHH*-$[RuLu(L1)_3]^{5+}$ on the NMR timescale (see Figure 1 for numbering). The unusual shielding of the aromatic protons $H^6$ and $H^9$ is diagnostic for the helical wrapping of the strands, which puts these protons in the shielding region of the neighbouring connected benzimidazole rings, as previously established for the analogous diamagnetic d–f helicates *HHH*-$[ZnLu(L1)_3]^{5+}$,[32] *HHH*-$[FeLu(L1)_3]^{5+}$[21] and *HHH*-$[CoLu(L1)_3]^{6+}$.[8]

The electronic absorption spectrum of *HHH*-$[RuLu(L1)_3]^{5+}$ in ethanol/methanol (4:1) (Figure S3a, Supporting Information) shows the $^1$MLCT transition centred at 21 100 $cm^{-1}$ as similarly observed for *fac*-$[Ru(L2)_3]^{3+}$ (Table 3), while the emission of the $^3$MLCT excited state, observed upon excitation of the $^1$MLCT transition, is slightly blue-shifted by 385 $cm^{-1}$ (Table 3; Figure S3b,c, Supporting Information). This suggests that the complexation of $Lu^{III}$ in the distal nine-coordination site affects the stereoelectronic properties of the pseudo-octahedral $Ru^{II}$ site in *HHH*-$[RuLu(L1)_3]^{5+}$ only very slightly. However, the lifetime of the triplet charge-transfer state ($\tau(^3MLCT) = 0.242(5)$ μs) is fivefold longer than that measured for *fac*-$[Ru(L2)_3]^{3+}$ at 296 K, while these lifetimes remain comparable at low temperature ($\tau(^3MLCT) = 2.0(1)$ μs for *HHH*-$[RuLu(L1)_3]^{5+}$ and $\tau(^3MLCT) = 3.2(1)$ μs for *fac*-$[Ru(L2)_3]^{2+}$ at 77 K; Table 3). The quantum yields follow the same trend and we tentatively assign this beneficial effect in the bimetallic helicate to a slightly larger separation $\Delta E = E(d\text{–}d) - E(^3MLCT)$ induced by a small distortion of the $Ru^{II}$ coordination sphere resulting from the complexation of $Lu^{III}$ in the neigh-

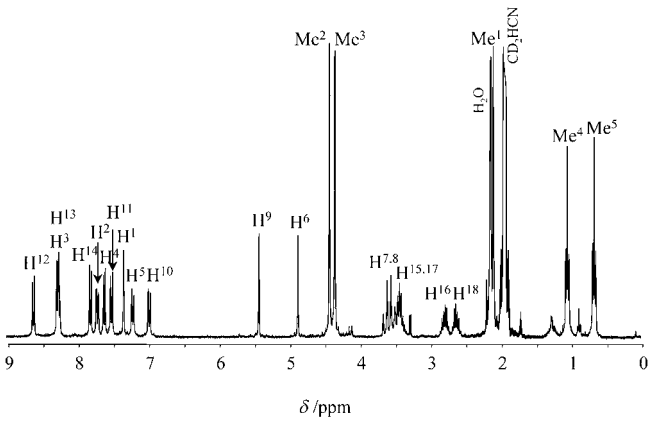


Figure 8. $^1H$ NMR spectrum of *HHH*-$[RuLu(L1)_3]^{5+}$ ($CD_3CN$, 298 K; numbering as in Figure 1).

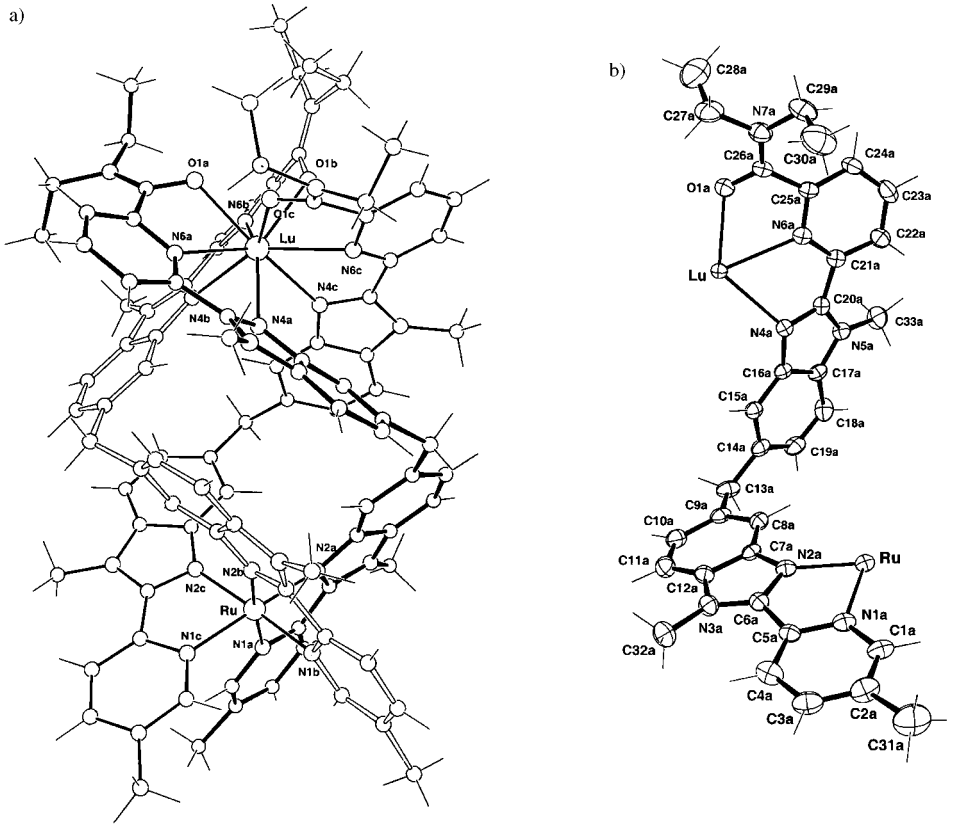


Figure 9. a) Perspective view of *HHH*-$[RuLu(L1)_3]^{5+}$ perpendicular to the pseudo-$C_3$ axis in the crystal structure of **6**, and b) atomic numbering scheme of strand a (ellipsoids are represented at the 40% probability level).

 © 2004 Wiley-VCH Verlag GmbH & Co. KGaA, Weinheim 

bouring site. Finally, fragile monocrystals suitable for X-ray diffraction analysis are obtained when half a triflate anion is replaced with $Cl^-$ to give *HHH*-$[RuLu(L1)_3](CF_3SO_3)_{4.5}Cl_{0.5}\cdot 2.5\,CH_3OH$ (**6**).

**Crystal and molecular structure of *HHH*-$[RuLu(L1)_3](CF_3SO_3)_{4.5}Cl_{0.5}\cdot 2.5\,CH_3OH$ (6)**: The crystal structure of **6** consists of triple-stranded cations *HHH*-$[RuLu(L1)_3]^{5+}$ together with disordered ionic triflate and chloride anions, and non-coordinated methanol molecules (see Experimental Section). The wrapping of the ligands results from successive torsions around the interaromatic C–C bonds, and around the central methylene unit as previously described for the analogous d–f bimetallic helicates *HHH*-$[ZnEu(L1)_3]^{5+}$,[32] *HHH*-$[FeLa(L1)_3]^{5+}$,[21] *HHH*-$[CrLu(L1)_3]^{6+}$[9] and *HHH*-$[CoLu(L1)_3]^{6+}$.[8] Selected bond lengths and bond angles for *HHH*-$[RuLu(L1)_3]^{5+}$ are collected in Table 4, while Figure 9 displays its molecular structure together with the atomic numbering scheme.

The similarity of the Lu–N and Lu–O bond lengths in *HHH*-$[RuLu(L1)_3]^{5+}$ and *HHH*-$[CoLu(L1)_3]^{6+}$[8] indicates that the complexation of the large low-spin $d^6$ $Ru^{II}$ ion (we calculate $R_{Ru}^{CN=6}=0.595$ Å in **6** according to Shannon's definition and $r(N)=1.46$ Å)[33] does not induce significant mechanical constraints around $Lu^{III}$ compared with the alternative complexation of the smaller $Co^{III}$ ion ($R_{Co}^{CN=6}=0.545$ Å).[33] The detailed geometrical analysis using the angles $\phi$, $\theta_i$ and $\omega_{ij}$ for the pseudo-tricapped trigonal prismatic $Lu^{III}$ site[8] shows only minor differences between *HHH*-$[RuLu(L1)_3]^{5+}$ and *HHH*-$[CoLu(L1)_3]^{6+}$ (Table S3, Supporting Information). However, the related analysis performed on the pseudo-octahedral $Ru^{II}$ and $Co^{III}$ sites highlights a slightly smaller twist of the the bidentate binding units around $Ru^{II}$ ($\omega_{ij}$(intraligand) = 52.9–54.5° compared with 56–57° around $Co^{III}$ in *HHH*-$[CoLu(L1)_3]^{6+}$; Table S4, Supporting Information). This translates into a larger helical pitch $P_{12}=d(F_1–F_2)/(\alpha/360)=13.35$ Å for the helical portion defined by the two facial planes $F_1$ (N1a,N1b,N1c) and $F_2$ (N2a,N2b,N2c) ($P_{12}=13.11$ Å in *HHH*-$[CoLu(L1)_3]^{6+}$,

Table 4. Selected bond lengths [Å] and bond angles [°] in $[RuLu(L1)_3](CF_3SO_3)_{4.5}Cl_{0.5}\cdot 2.5\,CH_3OH$ (**6**) and $[CoLu(L1)_3](CF_3SO_3)_6(CH_3CN)_2(H_2O)$.

| $[RuLu(L1)_3](CF_3SO_3)_{4.5}Cl_{0.5}\cdot 2.5\,CH_3OH$ (**6**) | | | | $[CoLu(L1)_3](CF_3SO_3)_6(CH_3CN)_2(H_2O)$[a] | | | |
|---|---|---|---|---|---|---|---|
| | ligand a | ligand b | ligand c | | ligand a | ligand b | ligand c |
| Lu···Ru | 9.0794(9) | – | – | Lu···Co | 9.234(2) | – | – |
| Lu–O1 | 2.345(5) | 2.284(5) | 2.326(4) | Lu–O1 | 2.316(5) | 2.340(5) | 2.339(5) |
| Lu–N4 | 2.534(6) | 2.469(6) | 2.514(5) | Lu–N4 | 2.474(5) | 2.516(6) | 2.495(6) |
| Lu–N6 | 2.518(4) | 2.531(5) | 2.515(4) | Lu–N6 | 2.526(6) | 2.508(6) | 2.518(6) |
| Ru–N1 | 2.064(6) | 2.060(5) | 2.055(5) | Co–N1 | 1.955(6) | 1.956(6) | 1.962(6) |
| Ru–N2 | 2.051(5) | 2.044(5) | 2.057(5) | Co–N2 | 1.929(6) | 1.925(6) | 1.914(6) |
| Bite angles | | | | | | | |
| O1-Lu-N4 | 128.2(1) | 128.7(2) | 129.6(2) | O1-Lu-N4 | 128.3(2) | 130.2(2) | 128.0(2) |
| O1-Lu-N6 | 63.8(2) | 64.2(2) | 65.2(1) | O1-Lu-N6 | 63.3(3) | 65.9(2) | 64.1(2) |
| N4-Lu-N6 | 64.5(2) | 64.5(2) | 64.7(2) | N4-Lu-N6 | 65.1(2) | 64.6(2) | 64.0(2) |
| N1-Ru-N2 | 77.8(2) | 77.5(2) | 77.9(2) | N1-Co-N2 | 83.2(2) | 83.1(2) | 82.1(2) |
| | | | | N-Co-N | | | |
| N-Ru-N | | | | | | | |
| N1a-Ru-N1b | 98.7(2) | N2a-Ru-N2b | 99.8(2) | N1a-Co-N1b | 94.8(2) | N2a-Ru-N2b | 93.6(2) |
| N1a-Ru-N2b | 175.7(2) | N2a-Ru-N2c | 99.3(2) | N1a-Co-N2b | 176.2(2) | N2a-Ru-N2c | 97.6(2) |
| N1a-Ru-N2c | 85.0(2) | N1b-Ru-N1c | 97.7(2) | N1a-Co-N2c | 88.2(2) | N1b-Ru-N1c | 93.9(2) |
| N1a-Ru-N1c | 95.0(2) | N1b-Ru-N2c | 174.5(2) | N1a-Co-N1c | 95.4(2) | N1b-Ru-N2c | 175.2(2) |
| N2a-Ru-N1b | 85.5(2) | N2b-Ru-N1c | 87.5(2) | N2a-Co-N1b | 86.5(2) | N2b-Ru-N1c | 87.8(2) |
| N2a-Ru-N1c | 172.5(2) | N2b-Ru-N2c | 99.0(2) | N2a-Co-N1c | 178.6(2) | N2b-Ru-N2c | 94.1(2) |
| | | | | N-Lu-N | | | |
| N-Lu-N | | | | | | | |
| N4a-Lu-N4b | 88.3(2) | N6a-Lu-N6b | 119.5(2) | N4a-Lu-N4b | 80.5(2) | N6a-Lu-N6b | 114.8(2) |
| N4b-Lu-N4c | 82.7(2) | N6b-Lu-N6c | 117.4(2) | N4b-Lu-N4c | 86.2(2) | N6b-Lu-N6c | 124.0(2) |
| N4a-Lu-N4c | 83.9(2) | N6a-Lu-N6c | 121.5(2) | N4a-Lu-N4c | 86.9(2) | N6a-Lu-N6c | 119.7(2) |
| N4a-Lu-N6c | 74.7(2) | N4a-Lu-N6b | 148.0(2) | N4a-Lu-N6c | 76.1(2) | N4a-Lu-N6b | 142.2(2) |
| N6a-Lu-N4b | 75.6(2) | N4b-Lu-N6c | 144.3(2) | N6a-Lu-N4b | 74.0(2) | N4b-Lu-N6c | 142.6(2) |
| N6b-Lu-N4c | 76.5(2) | N6a-Lu-N4c | 141.6(2) | N6b-Lu-N4c | 77.2(2) | N6a-Lu-N4c | 147.6(2) |
| | | | | O-Lu-N | | | |
| O-Lu-N | | | | | | | |
| N4a-Lu-O1b | 139.9(2) | N4a-Lu-O1c | 79.1(2) | N4a-Lu-O1b | 143.8(2) | N4a-Lu-O1c | 82.8(2) |
| N6a-Lu-O1b | 132.1(2) | N6a-Lu-O1c | 67.4(2) | N6a-Lu-O1b | 134.1(2) | N6a-Lu-O1c | 66.7(2) |
| N6b-Lu-O1c | 132.7(2) | N4b-Lu-O1c | 142.8(1) | N6b-Lu-O1c | 133.7(2) | N4b-Lu-O1c | 140.7(2) |
| O1a-Lu-N6b | 67.5(2) | O1a-Lu-N4b | 82.7(2) | O1a-Lu-N6b | 65.4(2) | O1a-Lu-N4b | 85.5(2) |
| O1a-Lu-N4c | 144.1(2) | O1a-Lu-N6c | 132.4(2) | O1a-Lu-N4c | 141.6(2) | O1a-Lu-N6c | 131.8(2) |
| O1b-Lu-N4c | 86.1(2) | O1b-Lu-N6c | 65.9(2) | O1b-Lu-N4c | 78.1(2) | O1b-Lu-N6c | 67.7(2) |
| | | | | O-Lu-O | | | |
| O-Lu-O | | | | | | | |
| O1a-Lu-O1b | 77.9(2) | O1b-Lu-O1c | 77.9(2) | O1a-Lu-O1b | 78.9(2) | O1b-Lu-O1c | 81.1(2) |
| O1a-Lu-O1c | 78.3(2) | – | – | O1a-Lu-O1c | 77.5(2) | – | – |

[a] Taken from ref. [8b].


© 2004 Wiley-VCH Verlag GmbH & Co. KGaA, Weinheim

Table 5).[8] The latter effect contrasts with the nonbonded Ru···Lu distance in *HHH*-$[RuLu(L1)_3]^{5+}$ (9.0794(9) Å), which is indeed shorter than the analogous Co···Lu distance reported for *HHH*-$[CoLu(L1)_3]^{6+}$ (9.234(2) Å),[8] and which may be ascribed to the increased wrapping (that is, a smaller helical pitch) characterizing the large intermetallic helical portion $F_2$–$F_3$ in *HHH*-$[RuLu(L1)_3]^{5+}$ (Table 5). Consequently, the two triple-helical complexes *HHH*-$[RuLu(L1)_3]^{5+}$ and *HHH*-$[CoLu(L1)_3]^{6+}$ cannot be strictly superimposed (Figure S4, Supporting Information).

Table 5. Helical pitches $P_{ij}$, linear distances $d(F_i–F_j)$ and average twist angles $\alpha_{ij}$ along the pseudo-$C_3$ axis[a] in the crystal structures of $[RuLu(L1)_3](CF_3SO_3)_{4.5}Cl_{0.5}\cdot 2.5\,CH_3OH$ (**6**) and $[CoLu(L1)_3](CF_3SO_3)_6(CH_3CN)_2(H_2O)$.

| | *HHH*-$[RuLu(L1)_3]^{5+}$ | | | *HHH*-$[CoLu(L1)_3]^{6+}$[b] | | |
|---|---|---|---|---|---|---|
| | $d(F_i–F_j)$ [Å] | $\alpha_{ij}$ [°][c] | $P_{ij}$ [Å] | $d(F_i–F_j)$ [Å] | $\alpha_{ij}$ [°] | $P_{ij}$ [Å] |
| $F_1$–$F_2$[d] | 2.00 | 54 | 13.35 | 2.04 | 56 | 13.11 |
| $F_2$–$F_3$ | 6.46 | 117 | 19.86 | 6.66 | 117 | 20.49 |
| $F_3$–$F_4$ | 1.75 | 52 | 12.06 | 1.75 | 52 | 12.11 |
| $F_4$–$F_5$ | 1.41 | 58 | 8.72 | 1.40 | 58 | 8.68 |
| $F_1$–$F_5$ | 11.62 | 281 | 14.88 | 11.85 | 284 | 15.02 |
| Lu···M | 9.0794(9) | – | – | 9.234(2) | – | – |

[a] Each helical portion $F_1$–$F_2$, $F_2$–$F_3$, $F_3$–$F_4$ and $F_4$–$F_5$ is characterised by 1) a linear extension $d(F_i–F_j)$ defined by the separation between the facial planes, 2) an average twist angle $\alpha_{ij}$ defined by the angular rotation between the projections of N*i* and N*j* (or O*j*) belonging to the same ligand strand onto an intermediate plane passing through the metal (or the midpoint X in Scheme 2*)* and 3) its pitch $P_{ij}$ defined as the ratio of axial over angular progressions along the helical axis $P_{ij}=d(F_i–F_j)/(\alpha_{ij}/360)$ ($P_{ij}$ corresponds to the length of a cylinder containing a single turn of the helix defined by geometrical characteristics $d(F_i–F_j)$ and $\alpha_{ij}$).[9] [b] Taken from refs. [8b] and [9]. [c] $\alpha_{ij}$ are given as $C_3$ average values. [d] $F_1$: N1a, N1b, N1c; $F_2$: N2a, N2b, N2c; $F_3$: N4a, N4b, N4c; $F_4$: N6a, N6b, N6c; $F_5$: O1a, O1b, O1c (see Scheme 2).

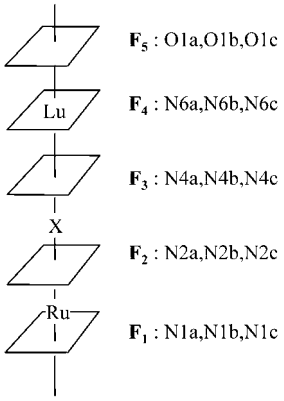


Scheme 2. Helical portions $F_i$–$F_j$ (see Table 5).

The pseudo-octahedral $Ru^{II}$ coordination sphere in *HHH*-$[RuLu(L1)_3]^{5+}$ shows that the three bidentate benzimidazol-2-ylpyridine units adopt a facial arrangement at odds with the molecular structure of *mer*-$[Ru(L3)_3]^{2+}$ (Figure 9). Interestingly, both the Ru–N1(pyridine) bond lengths (average: 2.060(5) Å; Table 4) and the Ru–N2(benzimidazole) bonds (average: 2.051(7) Å; Table 4) are shorter than those measured in *mer*-$[Ru(L3)_3]^{2+}$, which implies that the complexation of $Lu^{III}$ constrains the bidentate binding to be closer to the $Ru^{II}$ ion. This is in line with the increased ligand field in *HHH*-$[RuLu(L1)_3]^{5+}$ suggested by our photophysical data (lifetimes and quantum yields). Finally, the triple-stranded *HHH*-$[RuLu(L1)_3]^{5+}$ ions are packed into columns along the [111] direction, thus providing a pseudo-hexagonal arrangement in the crystal of **6** (Figure S5, Supporting Information). In each column, two successive helices are related by an inversion centre leading to intermolecular Lu···Lu and Ru···Ru distances of 12.9536(9) and 9.1632(11) Å respectively.

## Conclusion

To the best of our knowledge, the thermodynamic self-assembly of the single-stranded bimetallic helicate $[(terpy)Ru(quinquepyridine)Ru(terpy)Cl]^{3+}$ is the only previously reported event in which $Ru^{II}$ has been tentatively used as a "labile" partner in the formation of helicates.[34] However, no yield was reported and the final complex was obtained upon reduction of a nonisolated $Ru^{III}$ precursor, which prevents rationalisation of the chemical mechanism. Another attempt provided a hexameric $Ru^{II}$ wheel from the $Ru^{III}$ precursor, but again it is not clear which oxidation state is involved in the thermodynamic equilibria.[13b] In this contribution, we have demonstrated that the kinetics of the *fac*-$[Ru(benzimidazol\text{-}2\text{-}ylpyridine)_3]^{2+}$⇌*mer*-$[Ru(benzimidazol\text{-}2\text{-}ylpyridine)_3]^{2+}$ isomerisation process depends on solvent polarity and on the substitution of the benzimidazole ring. Although the chemical origins of these effects await complete variable-temperature thermodynamic and kinetic studies, their exploitation in the self-assembly of heterobimetallic d–f helicates has led to the first isolation of a triple-stranded Ru-containing helicate, $[RuLu(L1)_3]^{5+}$. This opens interesting perspectives for using $[Ru(\alpha,\alpha'\text{-diimine})_3]^{2+}$ as sensitisers for ultimate near-infrared emissions of distal 4f-block ions (Ln = Nd, Er, Yb),[3] but the specific photophysical properties of the $[Ru(benzimidazol\text{-}2\text{-}ylpyridine)_3]^{2+}$ chromophore is not ideal (short $\tau(^3MLCT)$ lifetimes and low quantum yields), because interactions with low-energy excited d–d states provide efficient thermally activated pathways for nonradiative deactivation. This situation is not desperate, however, since such deleterous effects can be removed either by the connection of π-attracting[35a] or σ-donating[35b] groups to the aromatic rings, which increases the ligand-field strength without significantly affecting the energy of the MLCT states. Finally, the comparison of the velocities of the *fac*-$[M(benzimidazol\text{-}2\text{-}ylpyridine)_3]^{2+}$⇌*mer*-$[M(benzimidazol\text{-}2\text{-}ylpyridine)_3]^{2+}$ isomerisation processes for M = $Ru^{II}$ (a typical inert d-block cation) with M = $Zn^{II}$ (a typical labile d-block cation) is very informative. Variable-temperature NMR data recorded for $[Zn(L2)_3]^{2+}$ and $[Zn(L3)_3]^{2+}$ in $CD_3CN$ show an average $D_{3h}$ symmetry at room temperature compatible with fast *fac*⇌*mer* isomerisation on the NMR timescale (that is, in the millisecond range; Figure S6, Supporting Information). Separated signals are only ob-

 © 2004 Wiley-VCH Verlag GmbH & Co. KGaA, Weinheim 

served at the lowest accessible temperature (233 K), and we can conclude that the assembly of the d–f helicates $[MLn(L1)_3]^{5+}$ can be performed successfully for noncovalent tripods whose lability changes by more than six orders of magnitude (that is, from the millisecond (M = Zn) to the hour (M = Ru) range).

## Experimental Section

**Solvents and starting materials**: These were purchased from Fluka AG (Buchs, Switzerland) and used without further purification unless otherwise stated. Acetonitrile, dichloromethane and *N*,*N*-dimethylformamide were distilled from $CaH_2$. The ligands 2-{6-[*N*,*N*-diethylcarboxamido]pyridin-2-yl}-1,1′-dimethyl-5,5′-methylene-2′-(5-methylpyridin-2-yl)bis[1*H*-benzimidazole] (L1),[32] 5-methyl-(1-methylbenzimidazol-2-yl)pyridine (L2),[15] 6-methylpyridine-2-carboxylic acid,[32] $[Ru(dmso)_4Cl_2]$[36] and $Na_2Sb_2[(+)\text{-}C_4O_6H_2]_2\cdot 5H_2O$[4a] were prepared according to literature procedures. The triflate salt $Lu(CF_3SO_3)_3\cdot 1.4H_2O$ was prepared from the corresponding oxide (Rhodia, 99.99%).[37] The Lu content of solid salts was determined by complexometric titrations with Titriplex III (Merck) in the presence of urotropine and xylene orange.[38]

**Preparation of benzyl(2-nitrophenyl)amine**: A mixture of 1-chloro-2-nitrobenzene (10 g, 0.0634 mol) and benzylamine (134 g, 1.25 mol) was stirred at 100 °C for 24 h in an autoclave. The orange solution was poured into water (80 mL) and extracted with dichloromethane (3 × 200 mL). The combined organic layers were dried over $MgSO_4$ and evaporated. The excess of benzylamine was removed by vacuum distillation ($5\times 10^{-2}$ bar, 30 °C), and the resulting orange solid purified by column chromatography (silica gel, $CH_2Cl_2$) to give 10.5 g (46.1 mmol, yield 73%) of benzyl(2-nitrophenyl)amine as an orange solid. M.p. = 72 °C. $^1$H NMR ($CDCl_3$): $\delta$ = 8.40 (br s, 1H, N*H*), 8.15 (dd, $J^3$ = 8 Hz, $J^4$ = 1 Hz, 1H), 7.25–7.35 (m, 6H), 6.75 (d, $J^3$ = 8 Hz, 1H), 6.60 (dt, $J^3$ = 8 Hz, $J^4$ = 1 Hz, 1H), 4.58 ppm (d, $J^3$ = 6 Hz, 2H); $^{13}$C NMR ($CDCl_3$): $\delta$ = 145.1, 137.2, 136.1, 132.0, 128.8, 127.6, 127.0, 126.7, 115.6, 114.1, 47.0 ppm; EI-MS: *m*/*z*: 228 [$M^+$]; elemental analysis calcd (%) for $C_{13}H_{12}N_2O_2$: C 68.41, H 5.30, N 12.27; found: C 68.50, H 5.27, N 12.35.

**Preparation of the [benzyl(2-nitrophenyl)]amide of 5-methylpyridine-2-carboxylic acid**: A mixture of 6-methylpyridine-2-carboxylic acid (1 g, 7.29 mmol), thionyl chloride (5.2 mL, 72.9 mmol) and DMF (300 μL) was refluxed for 90 min in dry dichloromethane (100 mL). The mixture was evaporated and dried under vacuum for 1 h. The resulting dark green solid was dissolved in dichloromethane (50 mL) and added dropwise to a solution of benzyl(2-nitrophenyl)amine (1.80 g, 7.9 mmol) and triethylamine (11 mL, 79 mmol). The solution was refluxed for 12 h under an inert atmosphere. After evaporation, the green residue was partitioned between dichloromethane (200 mL) and half-saturated aqueous $NH_4Cl$ solution (200 mL). The aqueous phase was extracted with dichloromethane (3 × 150 mL), then the combined organic layers were dried ($MgSO_4$) and evaporated. The crude brown oil was purified by column chromatography (silica gel, $CH_2Cl_2$/MeOH (100:0→98:2)) to give (1.7 g, 4.9 mmol; yield 67%) of 5-methylpyridine-2-carboxylic acid [benzyl(2-nitrophenyl)]amide as a pale orange solid. M.p. = 80 °C; $^1$H NMR ($CDCl_3$): $\delta$ = 7.87 (s, 1H), 7.82 (dd, $J^3$ = 8 Hz, $J^4$ = 1 Hz, 1H), 7.68 (dd, $J^3$ = 8 Hz, 1H), 7.39 (dd, $J^3$ = 8 Hz, $J^4$ = 1 Hz, 1H), 7.31–7.22 (m, 7H), 6.90 (dd, $J^3$ = 8 Hz, $J^4$ = 1 Hz, 1H), 5.71 (d, $J^2$ = 15 Hz, 1H), 4.45 (d, $J^2$ = 15 Hz, 1H), 2.16 ppm (s, 3H); $^{13}$C NMR ($CDCl_3$): $\delta$ = 167.7, 150.0, 148.0, 146.8, 137.4, 137.2, 136.7, 134.8, 133.1, 132.3, 129.6, 129.0, 128.7, 128.0, 125.2, 124.3, 54.1, 18.3 ppm; EI-MS: *m*/*z*: 347 [$M^+$]; elemental analysis calcd (%) for $C_{20}H_{17}N_3O_3$: C 69.15, H 4.93, N 12.10; found: C 69.30, H 5.10, N 12.15.

**Preparation of 5-methyl(1-benzylbenzimidazol-2-yl)pyridine (L3)**: The [benzyl(2-nitrophenyl)]amide of 5-methylpyridine-2-carboxylic acid (600 mg, 1.7 mmol) was dissolved in ethanol (120 mL) containing distilled water (40 mL), concentrated HCl (4 mL, 37%) and activated iron (2 g, 36 mmol). The solution was refluxed for 12 h under a nitrogen atmosphere. The excess of metallic iron was removed by filtration, the ethanol was evaporated and a solution of $Na_2H_2EDTA$ (20 g, 55 mmol, in 100 mL of water) was added. The pH was adjusted to 9 with ammonium hydroxide, and the aqueous phase was extracted with dichloromethane (3 × 100 mL). The combined organic phases were dried over $MgSO_4$ and the solvent was evaporated. The resulting solid was recrystallised from dichloromethane/hexane (50:50) to give L3 (460 mg, 1.54 mmol; yield 90%) as a white microcrystalline powder. M.p. = 120 °C; $^1$H NMR ($CDCl_3$): $\delta$ = 8.41 (dd, $J^3$ = 8 Hz, $J^4$ = 1 Hz, 1H), 8.30 (d, $J^3$ = 9 Hz, 1H), 7.81 (dd, $J^3$ = 8 Hz, $J^4$ = 1 Hz, 1H), 7.60 (dd, $J^3$ = 8 Hz, $J^4$ = 1 Hz, 1H), 7.10–7.32 (m, 7H), 6.15 (s, 2H), 2.34 ppm (s, 3H); $^{13}$C NMR ($CDCl_3$): $\delta$ = 150.3, 149.1, 148.8, 148.0, 142.9, 137.9, 137.7, 137.5, 136.9, 133.8, 128.6, 127.3, 126.9, 124.3, 123.4, 122.8, 120.0, 110.8, 49.0, 18.5 ppm; EI-MS: *m*/*z*: 299 [$M^+$]; elemental analysis calcd (%) for $C_{20}H_{17}N_3$: C 80.24, H 5.72, N 14.04; found: C 80.30, H 5.65, N 14.17.

**Preparation of $[Ru(dmso)_5(H_2O)](CF_3SO_3)_2\cdot H_2O$**: $[Ru(dmso)_4(Cl)_2]$ (300 mg, 0.62 mmol) and $Ag(CF_3SO_3)$ (319 mg, 1.24 mmol, 2.1 equiv) were dissolved in DMSO/acetone (2:1, 6.5 mL). After 1 h of stirring at RT, the solution was filtered to remove AgCl and acetone (50 mL) was added to induce precipitation. After 6 h at 4 °C, $[Ru(dmso)_5(H_2O)](CF_3SO_3)_2\cdot H_2O$ (310 mg, 0.47 mmol; yield 70%) was isolated by filtration as a pale yellow powder. ESI-MS: *m*/*z*: 257 $[Ru(dmso)_5(H_2O)]^{2+}$; elemental analysis calcd (%) for $[Ru(dmso)_5(H_2O)](CF_3SO_3)_2\cdot H_2O$: C, 17.50; H, 4.12. found: C, 17.51; H, 4.11.

**Preparation of $[Ru(L2)_3](ClO_4)_2\cdot 2H_2O$**: A mixture of L2 (100 mg, 0.45 mmol) and $[Ru(dmso)_4Cl_2]$ (72.5 mg, 0.15 mmol) was refluxed in ethanol (20 mL) for 24 h. The solution turned deep red and was concentrated to a final volume of about 10 mL. Diethyl ether was added to induce precipitation, and a red solid (90 mg) was collected by filtration and redissolved in water (18 mL). A saturated aqueous solution of sodium perchlorate was added until precipitation occurred. The crude product was extracted with dichloromethane (2 × 10 mL), and the red solid was separated by filtration and precipitated from acetonitrile/diethyl ether to give $[Ru(L2)_3](ClO_4)_2\cdot 2H_2O$ (81 mg, 0.084 mmol; yield 56%) as a 3:1 mixture of *mer*-$[Ru(L2)_3](ClO_4)_2\cdot 2H_2O$ and *fac*-$[Ru(L2)_3](ClO_4)_2\cdot 2H_2O$; ESI-MS: *m*/*z*: 385 $[Ru(L2)_3]^{2+}$; elemental analysis calcd (%) for $C_{42}H_{39}N_9O_8Cl_2Ru\cdot 2H_2O$: C 50.20, H 4.25, N 12.54; found: C 50.14, H 4.12, N 12.68.

**Separation of *mer*-$[Ru(L2)_3](ClO_4)_2\cdot 2H_2O$ (1) and *fac*-$[Ru(L2)_3](ClO_4)_2\cdot 2H_2O$ (2)**: In a typical experiment, a portion (50 mg) of the 3:1 mixture was dissolved in dichloromethane (1 mL) and extracted with an aqueous solution of $Na_2Sb_2[(+)\text{-}C_4O_6H_2]_2\cdot 5H_2O$ (1 mL, 0.1 mol L$^{-1}$). The aqueous phase was separated and sorbed onto a column (1.5 cm diameter and 1 m length) containing Sephadex C-25 (10 g) suspended in water. The elution was performed using an aqueous solution of $Na_2Sb_2[(+)\text{-}C_4O_6H_2]\cdot 5H_2O$ (0.1 mol L$^{-1}$). Two successive bands were collected separately. Precipitation with saturated aqueous $NaClO_4$ (1 mL) gave *mer*-$[Ru(L2)_3](ClO_4)_2\cdot 2H_2O$ (**1**, 34.5 mg; yield 69%) and *fac*-$[Ru(L2)_3](ClO_4)_2\cdot 2H_2O$ (**2**, 10 mg; yield 20%).

***mer*-$[Ru(L2)_3](ClO_4)_2\cdot 2H_2O$ (1)**: ESI-MS: *m*/*z*: 385 $[Ru(L2)_3]^{2+}$; elemental analysis calcd (%) for $C_{42}H_{39}N_9O_8Cl_2Ru\cdot 2H_2O$ (*mer*): C 50.20, H 4.25, N 12.54; found: C 50.14, H 4.18, N 12.69.

***fac*-$[Ru(L2)_3](ClO_4)_2\cdot 2H_2O$ (2)**: ESI-MS: *m*/*z*: 385 $[Ru(L2)_3]^{2+}$; elemental analysis calcd (%) for $C_{42}H_{39}N_9O_8Cl_2Ru\cdot 2H_2O$ (*fac*): C 50.20, H 4.25, N 12.54; found: C 50.17,H 4.14, N 12.62.

**Preparation of $[Ru(L3)_3](ClO_4)_2\cdot CH_3CN\cdot H_2O$**: A solution of L3 (100 mg, 0.34 mmol) and $[Ru(dmso)_4Cl_2]$ (56.6 mg, 0.11 mmol) in ethanol was refluxed for 24 h. Half of the solvent was removed by distillation and precipitation was induced by adding diethyl ether. After filtration, the residual red solid was dissolved in water (10 mL) and saturated aqueous $NaClO_4$ was added until a red solid was precipitated; it was collected by filtration. Precipitation from acetonitrile/diethyl ether gave $[Ru(L3)_3](ClO_4)_2\cdot CH_3CN\cdot H_2O$ (95 mg, 0.079 mmol; yield 72%) as a 3:1 mixture of *mer*-$[Ru(L3)_3](ClO_4)_2\cdot CH_3CN\cdot H_2O$ and *fac*-$[Ru(L3)_3](ClO_4)_2\cdot CH_3CN\cdot H_2O$. ESI-MS: *m*/*z*: 499.8 $[Ru(L3)_3]^{2+}$; elemental analysis calcd (%) for $C_{60}H_{51}N_9O_8Cl_2Ru\cdot CH_3CN\cdot H_2O$: C 59.23, H 4.49, N 11.14; found: C 59.30, H 4.55, N 11.21.

**Separation of *mer*-$[Ru(L3)_3](ClO_4)_2\cdot CH_3CN\cdot H_2O$ (3)**: In a typical experiment, a portion (50 mg) of the 3:1 mixture was dissolved in dichloromethane (1 mL) and extracted with an aqueous solution of $Na_2Sb_2[(+)\text{-}C_4O_6H_2]_2\cdot 5H_2O$ (1 mL, 0.1 mol L$^{-1}$). The aqueous phase was separated and sorbed onto a column (diameter 1.5 cm, length 1 m) containing Sephadex C-25 (10 g) suspended in water. The elution was performed using an aqueous solution of $Na_2Sb_2[(+)\text{-}C_4O_6H_2]\cdot 5H_2O$ (0.1 mol L$^{-1}$). A single band was collected and precipitated with saturated aqueous $NaClO_4$


© 2004 Wiley-VCH Verlag GmbH & Co. KGaA, Weinheim

(1 mL) to give *mer*-$[Ru(L3)_3](ClO_4)_2\cdot CH_3CN\cdot H_2O$ (**3**, 45 mg; yield 90%). ESI-MS: *m/z*: 499.6 $[Ru(L3)_3]^{2+}$; elemental analysis calcd (%) for $C_{60}H_{51}N_9O_8Cl_2Ru\cdot CH_3CN\cdot H_2O$: C 59.23, H 4.49, N 11.14; found: C 59.32, H 4.59, N 11.19. X-ray quality prisms of *mer*-$[Ru(L3)_3](ClO_4)_2$ (**4**) were obtained by slow diffusion of *tert*-butyl methyl ether into a concentrated solution of **3** in acetonitrile.

**Preparation of *HHH*-$[RuLu(L1)_3](CF_3SO_3)_5\cdot 2CH_3OH\cdot H_2O$ (5)**: Ligand L1 (100 mg, 0.183 mmol, 3 equiv) was suspended in ethanol (8 mL) under an inert atmosphere and $Lu(CF_3SO_3)_3\cdot 1.4H_2O$ (39.7 mg, 0.0612 mmol, 1 equiv) dissolved in ethanol (0.5 mL) was added. This mixture was stirred for 30 min, then solid $[Ru(dmso)_5(H_2O)](CF_3SO_3)_2\cdot H_2O$ (50.5 mg, 0.0612 mmol, 1 equiv) was added. The resulting mixture was refluxed for 6 h and then filtered to remove solid impurities. The solvent was distilled under vacuum, and a red solid was obtained. Recrystallisation from methanol/diethyl ether led to the formation of **5** (115 mg, 0.043 mmol; yield 70%). ESI-MS: *m/z*: 514.4 $(RuLu(L^1)_3(CF_3SO_3)]^{4+}$; elemental analysis calcd (%) for $[LuRu(L1)_3](CF_3SO_3)_5\cdot 2CH_3OH\cdot H_2O$: C, 46.56; H, 4.02; N, 10.76; found: C, 46.71; H, 4.11; N, 10.87.

**Preparation of *HHH*-$[RuLu(L1)_3](CF_3SO_3)_{4.5}Cl_{0.5}\cdot 2.5CH_3OH$ (6)**: The procedure described for **5** was followed, except for the use of $[Ru(dmso)_4(Cl)_2]$ (29.6 mg, 0.0612 mmol, 1 equiv). The resulting mixture was refluxed for 16 h and then filtered to remove solid impurities. The solvent was distilled under vacuum and a red solid was obtained. Diffusion of diethyl ether into a concentrated methanol solution of the complex led to *HHH*-$[RuLu(L1)_3]Cl_2(CF_3SO_3)_3\cdot 3CH_3OH\cdot 2H_2O$ (63 mg, 0.025 mmol; yield 40%). ESI-MS: *m/z*: 514.4 $[RuLu(L^1)_3(CF_3SO_3)]^{4+}$ elemental analysis calcd (%) for $[LuRu(L1)_3]Cl_2(CF_3SO_3)_3\cdot 3CH_3OH\cdot 2H_2O$: C, 46.90; H, 4.25; N, 10.77; found: C, 46.91; H, 4.23; N, 10.75%. Crystals of *HHH*-$[RuLu(L1)_3](CF_3SO_3)_{4.5}Cl_{0.5}\cdot 2.5CH_3OH$ (**6**) suitable for X-ray diffraction were obtained by layering pentane onto a solution of *HHH*-$[RuLu(L1)_3]Cl_2(CF_3SO_3)_3\cdot 3CH_3OH\cdot 2H_2O$ in methanol.

**Crystal structure determinations of *mer*-$[Ru(L3)_3](ClO_4)_2$ (4) and *HHH*-$[RuLu(L1)_3](CF_3SO_3)_{4.5}Cl_{0.5}\cdot 2.5CH_3OH$ (6)**: The crystal data, intensity measurements and structure refinements are collected in Table 6. The crystals were mounted on quartz fibre with protection oil. Cell dimensions and intensities were measured at 200 K on a Stoe IPDS diffractometer with graphite-monochromated $Mo_{K\alpha}$ radiation ($\lambda = 0.71073$ Å). Data were corrected for Lorentz and polarisation effects and for absorption. The structures were solved by direct methods (SIR97);[39] all other calculations were performed with the XTAL[40] system and ORTEP[41] programs.

***mer*-$[Ru(L3)_3](ClO_4)_2$ (4)**: The hydrogen atoms of the methyl groups were refined with restraints on bond lengths and bond angles, and blocked during the last cycle. The positions of the other hydrogen atoms were calculated. The perchlorate anion e was disordered and refined on two positions with population parameters of 0.8 and 0.2, and possessing a common position for the chlorine atom. The latter perchlorate ($PP = 0.2$) was refined with restraints on bond lengths and bond angles.

***HHH*-$[RuLu(L1)_3](CF_3SO_3)_{4.5}Cl_{0.5}\cdot 2.5CH_3OH$ (6)**: All the non-hydrogen atoms of the cation *HHH*-$[RuLu(L1)_3]^{5+}$ and the triflate anions d and e were refined with anisotropic displacement parameters. The triflates f and g were disordered and each was refined on two positions with population parameters of 0.7/0.3 (triflate f) and 0.5/0.5 (triflate g). The triflate h and two disordered chlorine atoms were located at about the same site and were refined with population parameters of 0.5, 0.35 and 0.15 respectively. Finally, 2.5 disordered methanol molecules were refined on four sites with population parameters of 1.0, 0.5, 0.5 and 0.5.

CCDC-229557 (**4**) and CCDC-229558 (**6**) contain the supplementary crystallographic data for this paper. These data can be obtained free of charge via www.ccdc.cam.ac.uk/conts/retrieving.html (or from the Cambridge Crystallographic Data Centre, 12 Union Road, Cambridge CB21EZ, UK; fax: (+44) 1223-336-033; or deposit@ccdc.cam.uk).

**Spectroscopic and analytical measurements**: $^1$H NMR spectra were recorded on a Broadband Varian Gemini 300 and on a Brucker DRX-500 spectrometer at 298 K. Chemical shifts are given in ppm versus TMS. Pneumatically assisted electrospray (ESI-MS) mass spectra were recorded from $10^{-4}$ mol L$^{-1}$ acetonitrile solutions on a Finnigan SSQ7000 instrument. Electronic spectra in the UV/Vis were recorded at 20°C from $10^{-4}$ mol L$^{-1}$ solutions in ethanol/methanol (4:1) with a Perkin–Elmer Lambda 900 spectrometer using quartz cells of 0.1 and 1 cm path length.

Table 6. Summary of crystal data, intensity measurements and structure refinement for *mer*-$[Ru(L3)_3](ClO_4)_2$ (**4**) and $[RuLu(L1)_3](CF_3SO_3)_{4.5}Cl_{0.5}\cdot 2.5CH_3OH$ (**6**).

| | **4** | **6** |
|---|---|---|
| formula | $RuC_{60}H_{51}N_9O_8Cl_2$ | $RuLuC_{106}H_{109}N_{21}O_{19}S_{4.5}F_{13.5}Cl_{0.5}$ |
| $M_r$ | 1198.2 | 2916.6 |
| colour | red | red |
| crystal system | monoclinic | triclinic |
| space group | $P2_1/n$ | – |
| $a$ [Å] | 12.2158(5) | 17.7294(13) |
| $b$ [Å] | 19.2808(10) | 19.2839(16) |
| $c$ [Å] | 23.3228(8) | 19.2890(13) |
| $\alpha$ [°] | 90 | 74.791(8) |
| $\beta$ [°] | 96.145(4) | 79.703(8) |
| $\gamma$ [°] | 90 | 69.673(9) |
| $V$ [Å$^3$] | 5461.7(4) | 5939.4(9) |
| $Z$ | 4 | 2 |
| $\rho_{calcd}$ [g cm$^{-3}$] | 1.457 | 1.496 |
| $\mu(Mo_{K\alpha})$ [mm$^{-1}$] | 0.451 | 1.137 |
| min/max transmission | 0.9117/0.9644 | 0.7695/0.8779 |
| crystal size [mm$^3$] | $0.084\times0.19\times0.32$ | $0.13\times0.21\times0.29$ |
| reflns measured | 76213 | 70437 |
| $2\theta$ range | $4.6° < 2\theta < 53.8°$ | $4.6° < 2\theta < 53.8°$ |
| unique reflns | 11325 | 23904 |
| reflns observed $[\lvert F_o\rvert > 4\sigma(F_o)]$ | 5994 | 13355 |
| parameters | 737 | 1500 |
| GOF | 1.31(1) | 1.59(1) |
| $\omega$ | $1/(\sigma^2(F_o)+0.00015(F_o)^2)$ | $1/(\sigma^2(F_o)+0.0001(F_o)^2)$ |
| $R$ | 0.036 | 0.044 |
| $R_\omega$ | 0.037 | 0.043 |
| min/max $\Delta\rho$ [e Å$^{-3}$] | −0.64/1.12 | −2.64/1.77 |

Emission spectra were recorded on a home-built set-up consisting of a single monochromator (Spex 270M) equipped with a nitrogen-cooled CCD camera (SpectrumOne Jobin Yvon-Spex) and appropriate collection optics. An Ar/Kr mixed-gas continuous-wave laser (Spectra Physics Stabilite 2108) tuned to the 457.5 nm line was used as excitation source. The emission quantum yields $\Phi$ were calculated using Equation (6), where x refers to the sample and r to the reference; $A$ is the absorbance at the excitation wavenumber used in the experiment, $I$ the intensity of the light, $n$ the refractive index and $D$ the integrated emitted intensity.

$$\frac{\Phi_x}{\Phi_r} = \frac{(1-\exp(-A_r(\nu))\, I_r(\nu)\, n_x^2\, D_x}{(1-\exp(-A_x(\nu))\, I_x(\nu)\, n_r^2\, D_r} \qquad (6)$$

$[Ru(2,2'bipyridine)_3](ClO_4)_2$ ($\Phi = 4.5\%$ in water) was used as reference for the determination of the quantum yields of complexes **1–5** in ethanol/methanol (4:1).[1a] For excited-state lifetime measurements, samples were excited at 532 nm with the second harmonic of a pulsed Nd:YAG laser (Quantel Brillant B, 20 Hz). Emission decay curves were recorded on a digital oscilloscope (Tektronix TDS 540B) using a fast photomultiplier tube (Hamamatsu TypH957-08). The time resolution of the set-up was 20 ns. Low-temperature glasses were produced in a custom-built sample cell inserted into a closed-cycle helium refrigeration system (Oxford Instruments CCC1100T). Cyclic voltammograms were recorded by using a BAS CV-50W potentiostat connected to a personal computer. A three-electrode system consisting of a stationary Pt disc working electrode, a Pt counter-electrode and a nonaqueous Ag/AgCl reference electrode was used. $[N(nBu)_4]ClO_4$ (0.1 mol L$^{-1}$ in MeCN) served as an inert electrolyte. The reference potential ($E^\ominus = -0.16$ V versus SCE) was standardised against $[Ru(bipy)_3](ClO_4)_2$ (bipy = 2,2′-bipyridyl).[23] The scan speed was 100 mV s$^{-1}$ and voltammograms were analysed according to established procedures.[23] Elemental analyses were performed by Dr. H. Eder from the Microchemical Laboratory of the University of Geneva.

 © 2004 Wiley-VCH Verlag GmbH & Co. KGaA, Weinheim 

## Acknowledgements

We are grateful to Mr. André Pinto and to Ms. Aurélie Maréchal for their technical assistance. Financial support from the National Research Programme 47 "Supramolecular Functional Materials", together with other grants from the Swiss National Science Foundation, is gratefully acknowledged.

[1] For reviews, see a) A. Juris, V. Balzani, F. Barigelletti, S. Campagna, P. Belser, A. von Zelewsky, *Coord. Chem. Rev.* **1988**, *84*, 85; b) E. C. Constable, *Adv. Inorg. Chem.* **1989**, *34*, 1; c) V. Balzani, A. Juris, S. Venturi, S. Campagna, S. Serroni, *Chem. Rev.* **1996**, *96*, 759; d) J. F. Endicott, B. H. Schlegel, M. J. Udin, D. S. Seniveratne, *Coord. Chem. Rev.* **2002**, *229*, 95.

[2] a) V. Balzani, S. Campagna, G. Denti, A. Juris, S. Serroni, M. Venturi, *Coord. Chem. Rev.* **1994**, *132*, 1; b) M. A. Haga, M. M. Ali, S. Koseki, K. Fujimoto, A. Yoshimura, K. Nozaki, T. Ohno, K. Nakajima, D. J. Stufkens, *Inorg. Chem.* **1996**, *35*, 3335; c) N. C. Fletcher, F. R. Keene, H. Vierborock, A. von Zelewsky, *Inorg. Chem.* **1997**, *36*, 1113; d) F. Vögtle, M. Plevoets, M. Nieger, G. C. Azzellini, A. Credi, L. De Cola, V. De Marchis, M. Venturi, V. Balzani, *J. Am. Chem. Soc.* **1999**, *121*, 6290; e) G. R. Newkome, E. He, C. N. Moorefield, *Chem. Rev.* **1999**, *99*, 1689; f) M. D. Ward, F. Barigelletti, *Coord. Chem. Rev.* **2001**, *216–217*, 127; g) J.-P. Launay, *Chem. Soc. Rev.* **2001**, *30*, 386; h) H. Yi, J. A. Crayston, J. T. S. Irvine, *Dalton Trans.* **2003**, 685.

[3] S. I. Klink, H. Keizer, F. C. J. M. van Veggel, *Angew. Chem.* **2000**, *112*, 4489; *Angew. Chem. Int. Ed.* **2000**, *39*, 4319.

[4] a) Y, Yoshikawa, K. Yamasaki, *Coord. Chem. Rev.* **1979**, *28*, 205; b) N. C. Fletcher, F. R. Keene, *J. Chem. Soc. Dalton Trans.* **1999**, 683; c) J. Lacour, V. Hebbe-Viton, *Chem. Soc. Rev.* **2003**, *32*, 373, and references therein.

[5] a) G. Orellana, A. Kirsh-DeMesmaeker, N. J. Turro, *Inorg. Chem.* **1990**, *29*, 882; b) G. Predieri, C. Vignali, G. Denti, S. Serroni, *Inorg. Chim. Acta* **1993**, *205*, 145; c) N. C. Fletcher, M. Nieuwenhuyzen, S. Rainey, *J. Chem. Soc. Dalton Trans.* **2001**, 2641, and references therein.

[6] a) M. Krejcik, S. Zalis, J. Klina, D. Sykora, W. Matheis, A. Klein, W. Kaim, *Inorg. Chem.* **1993**, *32*, 3362; b) T. J. Rutherford, D. A. Reitsma, F. R. Keene, *J. Chem. Soc. Dalton Trans.* **1994**, 3659; c) G. Tresoldi, S. Loschiavo, P. Piraino, *Inorg. Chim. Acta* **1997**, *254*, 381.

[7] N. C. Fletcher, M. Nieuwenhuyzen, R. Prabaharan, A. Wilson, *Chem. Commun.* **2002**, 1188.

[8] a) S. Rigault, C. Piguet, G. Bernardinelli, G. Hopfgartner, *Angew. Chem.* **1998**, *110*, 178; *Angew. Chem. Int. Ed.* **1998**, *37*, 169; b) S. Rigault, C. Piguet, G. Bernardinelli, G. Hopfgartner, *J. Chem. Soc. Dalton Trans.* **2000**, 4587.

[9] M. Cantuel, G. Bernardinelli, D. Imbert, J.-C. G. Bünzli, G. Hopfgartner, C. Piguet, *J. Chem. Soc. Dalton Trans.* **2002**, 1929.

[10] a) J. S. Lindsey, *New J. Chem.* **1991**, *15*, 153; b) J.-M. Lehn, *Supramolecular Chemistry*, VCH, Weinheim, **1995**; c) C. Piguet, G. Bernardinelli, G. Hopfgartner, *Chem. Rev.* **1997**, *97*, 2005.

[11] M. Cantuel, G. Bernardinelli, G. Muller, J. P. Riehl, C. Piguet, *Inorg. Chem.* **2004**, *43*, 1840.

[12] D. Imbert, M. Cantuel, J.-C. G. Bünzli, G. Bernardinelli, C. Piguet, *J. Am. Chem. Soc.* **2003**, *125*, 15698.

[13] a) D. P. Rillema, G. Allen, T. J. Meyer, D. Conrad, *Inorg. Chem.* **1983**, *22*, 1617; b) G. R. Newkome, T. J. Cho, C. N. Moorefield, R. Cush, P. S. Russo, L. A. Godinez, M. J. Saunders, P. Mohapatra, *Chem. Eur. J.* **2002**, *8*, 2946.

[14] M. H. W. Lam, S. T. C. Cheung, K.-M. Fung, W.-T. Wong, *Inorg. Chem.* **1997**, *36*, 4618.

[15] L. J. Charbonnière, A. F. Williams, C. Piguet, G. Bernardinelli, E. Rivara-Minten, *Chem. Eur. J.* **1998**, *4*, 485.

[16] C. Piguet, B. Bocquet, G. Hopfgartner, *Helv. Chim. Acta* **1994**, *77*, 931.

[17] P. J. Steel, F. Lahousse, D. Lerner, C. Marzin, *Inorg. Chem.* **1983**, *22*, 1488.

[18] A. B. Tamayo, B. D. Alleyne, P. I. Djurovich, S. Lamansky, I. Tsyba, N. H. Ho, R. Bau, M. E. Thompson, *J. Am. Chem. Soc.* **2003**, *125*, 7377.

[19] M. E. Starzak, *Mathematical Methods in Chemistry and* Physics, Plenum, New York, **1989**, Chapter 6, p. 289.

[20] C. Piguet, G. Bernardinelli, B. Bocquet, O. Schaad, A. F. Williams, *Inorg. Chem.* **1994**, *33*, 4112.

[21] C. Piguet, E. Rivara-Minten, G. Bernardinelli, J.-C. G. Bünzli, G. Hopfgartner, *J. Chem. Soc. Dalton Trans.* **1997**, 421.

[22] J. M. Harrowfield, A. N. Sobolev, *Aust. J. Chem.* **1994**, *47*, 763.

[23] A. J. Bard, L. R. Faulkner, *Electrochemical Methods, Fundamentals and Applications*, Wiley, New York, **1980**.

[24] a) J. E. Figard, J. D. Petersen, *Inorg. Chem.* **1978**, *17*, 1059; b) C. Malouf, P. C. Ford, *J. Am. Chem. Soc.* **1977**, *99*, 7213.

[25] G. Orellana, M. L. Quiroga, A. M. Braun, *Helv. Chim. Acta* **1987**, *70*, 2073.

[26] M. Haga, T. Tanaka, *Chem. Lett.* **1979**, 863.

[27] P. Xie, Y.-J. Chen, J. F. Endicott, M. J. Uddin, D. Seneviratne, P. G. McNamara, *Inorg. Chem.* **2003**, *42*, 5040.

[28] a) E. S. Dodsworth, A. B. P. Lever, *Chem. Phys. Lett.* **1985**, *119*, 61; b) E. S. Dodsworth, A. B. P. Lever, *Chem. Phys. Lett.* **1986**, *124*, 152; c) S. I. Gorelssky, V. Y. Kotov, A. B. P. Lever, *Inorg. Chem.* **1998**, *37*, 4584.

[29] F. Barigelletti, A. Juris, V. Balzani, P. Belser, A. von Zelewsky, *Inorg. Chem.* **1983**, *22*, 3335.

[30] C. K. Jørgensen, *Acta Chem. Scand.* **1955**, *9*, 1362.

[31] C. Edder, C. Piguet, G. Bernardinelli, J. Mareda, C. G. Bochet, J.-C. G. Bünzli, G. Hopfgartner, *Inorg. Chem.* **2000**, *39*, 5059.

[32] C. Piguet, J.-C. G. Bünzli, G. Bernardinelli, G. Hopfgartner, S. Petoud, O. Schaad, *J. Am. Chem. Soc.* **1996**, *118*, 6681.

[33] R. D. Shannon, *Acta Crystallogr. Sect A* **1976**, *32*, 751.

[34] C. J. Cathey, E. C. Constable, M. J. Hannon, D. A. Tocher, M. D. Ward, *J. Chem. Soc. Chem. Commun.* **1990**, 621.

[35] a) E. C Constable, A. M. W. Cargill Thompson, N. Armaroli, V. Balzani, M. Maestri, *Polyhedron* **1992**, *11*, 2707; b) M. Duati, S. Tasca, F. C. Lynch, H. Bohlen, J. G. Vos, S. Stagni, M. D. Ward, *Inorg. Chem.* **2003**, *42*, 8377, and references therein.

[36] I. P. Evans, A. Spencer, G. Wilkinson, *J. Chem. Soc. Dalton Trans.* **1973**, 204.

[37] J. F. Desreux, in *Lanthanide Probes in Life, Chemical and Earth Sciences* (Eds.: J.-C. G. Bünzli, G. R. Choppin), Elsevier, Amsterdam, **1989**, Chapter 2, p. 43.

[38] G. Schwarzenbach, *Complexometric Titrations*; Chapman and Hall, London, **1957**, p. 8.

[39] A. Altomare, M. C. Burla, M. Camalli, G. Cascarano, C. Giacovazzo, A. Guagliardi, A. G. G. Moliterni, G. Polidori, R. Spagna, *J. Appl. Crystallogr.* **1999**, *32*, 115.

[40] XTAL 3.2 User's Manual, (Eds.: S. R. Hall, H. D. Flack, J. M. Stewart, Universities of Western Australia, Maryland and Geneva, **1992**.

[41] C. K. Johnson, ORTEP II, Report ORNL-5138, Oak Ridge National Laboratory, Oak Ridge, TN, **1976**.

Received: January 29, 2004
Published online: May 26, 2004

 © 2004 Wiley-VCH Verlag GmbH & Co. KGaA, Weinheim 